

University of Groningen

Longitudinal gut microbiome changes in immune checkpoint blockade-treated advanced melanoma

Björk, Johannes R; Bolte, Laura A; Maltez Thomas, Andrew; Lee, Karla A; Rossi, Niccolo; Wind, Thijs T; Smit, Lotte M; Armanini, Federica; Asnicar, Francesco; Blanco-Miguez, Aitor

Published in:
Nature Medicine

DOI:
[10.1038/s41591-024-02803-3](https://doi.org/10.1038/s41591-024-02803-3)

IMPORTANT NOTE: You are advised to consult the publisher's version (publisher's PDF) if you wish to cite from it. Please check the document version below.

Document Version
Publisher's PDF, also known as Version of record

Publication date:
2024

[Link to publication in University of Groningen/UMCG research database](#)

Citation for published version (APA):

Björk, J. R., Bolte, L. A., Maltez Thomas, A., Lee, K. A., Rossi, N., Wind, T. T., Smit, L. M., Armanini, F., Asnicar, F., Blanco-Miguez, A., Board, R., Calbet-Llopart, N., Derosa, L., Dhomen, N., Brooks, K., Harland, M., Harries, M., Lorigan, P., Manghi, P., ... Weersma, R. K. (2024). Longitudinal gut microbiome changes in immune checkpoint blockade-treated advanced melanoma. *Nature Medicine*, 30, 785–796. <https://doi.org/10.1038/s41591-024-02803-3>

Copyright

Other than for strictly personal use, it is not permitted to download or to forward/distribute the text or part of it without the consent of the author(s) and/or copyright holder(s), unless the work is under an open content license (like Creative Commons).

The publication may also be distributed here under the terms of Article 25fa of the Dutch Copyright Act, indicated by the "Taverne" license. More information can be found on the University of Groningen website: <https://www.rug.nl/library/open-access/self-archiving-pure/taverne-amendment>.

Take-down policy

If you believe that this document breaches copyright please contact us providing details, and we will remove access to the work immediately and investigate your claim.

Downloaded from the University of Groningen/UMCG research database (Pure): <http://www.rug.nl/research/portal>. For technical reasons the number of authors shown on this cover page is limited to 10 maximum.

Longitudinal gut microbiome changes in immune checkpoint blockade-treated advanced melanoma

Received: 20 June 2023

Accepted: 3 January 2024

Published online: 16 February 2024

 Check for updates

A list of authors and their affiliations appears at the end of the paper

Multiple clinical trials targeting the gut microbiome are being conducted to optimize treatment outcomes for immune checkpoint blockade (ICB). To improve the success of these interventions, understanding gut microbiome changes during ICB is urgently needed. Here through longitudinal microbiome profiling of 175 patients treated with ICB for advanced melanoma, we show that several microbial species-level genome bins (SGBs) and pathways exhibit distinct patterns from baseline in patients achieving progression-free survival (PFS) of 12 months or longer (PFS ≥ 12) versus patients with PFS shorter than 12 months (PFS < 12). Out of 99 SGBs that could discriminate between these two groups, 20 were differentially abundant only at baseline, while 42 were differentially abundant only after treatment initiation. We identify five and four SGBs that had consistently higher abundances in patients with PFS ≥ 12 and < 12 months, respectively. Constructing a log ratio of these SGBs, we find an association with overall survival. Finally, we find different microbial dynamics in different clinical contexts including the type of ICB regimen, development of immune-related adverse events and concomitant medication use. Insights into the longitudinal dynamics of the gut microbiome in association with host factors and treatment regimens will be critical for guiding rational microbiome-targeted therapies aimed at enhancing ICB efficacy.

Immune checkpoint blockade (ICB) has revolutionized the field of oncology by prolonging the survival of patients with different tumor types at advanced stages¹. However, only a subset of patients responds to ICB, and the treatment can induce a variety of immune-related adverse events (irAEs), including colitis^{2,3}. Cross-sectional studies have assessed the gut microbiome before ICB initiation^{4–12}, but the field is hampered by a lack of consensus as different studies often report different microbial biomarkers of response⁴—a heterogeneity that is probably the result of many methodological, biological and/or clinical confounders but that also arises from the high intra- and inter-individual variation of the gut microbiome^{13–15}. Despite the lack of a thorough understanding of underlying mechanisms, multiple microbiome-directed clinical trials are ongoing in the oncoimmunology field, including fecal microbiota transplantation (FMT) trials¹⁶. To better interpret the findings from these trials and to increase our

understanding of gut microbiome dynamics more generally and in the context of ICB, there is an urgent need for longitudinal microbiome studies along the course of ICB treatment.

In this Article, we therefore describe the profiling of the gut microbiome (via shotgun metagenomics followed by MetaPhlan4¹⁷ and microbial metabolic (MetaCyc)¹⁸ analyses) at four time points during the first 12 weeks of treatment in a multicenter cohort comprising 175 patients treated with ICB for advanced melanoma (Extended Data Fig. 1). First, because patients received an immunotherapy infusion at each study visit (thus, the effect of ICB on the gut microbiome may increase as the treatment progresses), we hypothesize that many microbial abundances may increase or decrease over the treatment period. Second, because baseline abundances of several microbial taxa have already been shown to differ between ICB response and nonresponse, we further hypothesize that patients responding and not responding to

✉ e-mail: bjork.johannes@gmail.com; r.k.weersma@umcg.nl

Table 1 | Cohort characteristics at study entry

	PRIMM-UK (n=54)	PRIMM-NL (n=74)	Manchester (n=17)	Leeds (n=19)	Barcelona (n=11)	All cohorts (n=175)	P value
Age (years), median (range)	64 (19–94)	60 (21–85)	66 (38–87)	57 (35–88)	64 (37–88)	63 (19–94)	0.127
Sex (female), n (%)	19 (35)	37 (50)	7 (41)	7 (37)	5 (45)	75 (43)	0.530
BMI (kg m ⁻²), mean (range)	28.6 (18.83–47.66)	27.02 (15.43–40.74)	26.92 (18.99–40.40)	28.46 (20.90–38.57)	26.27 (20.96–36.08)	27.63 (15.43–47.66)	0.075
Metastatic stage, n (%)							0.006
Stage 3 unresectable	5 (9)	2 (3)	0 (0)	1 (5)	0 (0)	8 (5)	
Stage 4 M1a	12 (22)	7 (9)	5 (29)	3 (16)	4 (36)	31 (18)	
Stage 4 M1b	12 (22)	14 (19)	2 (12)	5 (26)	5 (45)	38 (22)	
Stage 4 M1c	20 (37)	23 (31)	8 (47)	7 (37)	2 (18)	60 (34)	
Stage 4 M1d	5 (9)	28 (38)	2 (12)	3 (16)	0 (0)	38 (22)	
BRAF mutant, n (%)	18 (33)	42 (57)	2 (12)	9 (47)	3 (27)	74 (42)	0.004
ECOG performance status ≥1, n (%)	36 (67)	17 (23)	8 (47)	2 (11)	1 (9)	64 (37)	1.729 × 10⁻⁶*
Outcomes following ICB							
PFS ≥12 months, n (%)	27 (50)	32 (43)	8 (47)	11 (58)	5 (45)	83 (47)	0.824
irAEs, n (%)	38 (70)	44 (59)	9 (53)	9 (47)	7 (64)	107 (61)	0.399
Colitis, n (%)	13 (24)	10 (14)	3 (18)	4 (21)	3 (27)	33 (19)	0.570
Treatment details							
ICB combination therapy (anti-CTLA-4/ anti-PD-1), n (%)	29 (54)	15 (20)	2 (12)	11 (58)	1 (9)	58 (33)	1.60 × 10⁻⁵*
Previous BRAF or MEK inhibition, n (%)	10 (19)	28 (38)	2 (12)	0 (0)	1 (9)	41 (23)	0.001*
PPI use at baseline, n (%)	13 (24)	24 (32)	4 (24)	6 (32)	1 (9)	48 (27)	0.495
Antibiotics use at baseline, n (%)	9 (17)	11 (15)	2 (12)	3 (16)	0 (0)	25 (14)	0.694

Baseline characteristics are presented as mean and s.d. or median (range) for continuous variables and as counts and percentages for categorical variables. χ^2 tests for categorical variables and two-sided Wilcoxon tests for continuous data were performed to calculate differences between cohorts. P values written in bold indicate nominally significant differences between cohorts ($P < 0.05$). *Statistical significance under a false discovery rate of 5%. UK, United Kingdom; NL, the Netherlands.

the treatment exhibit different patterns of microbial increase/decrease. To model this, we used a Bayesian regression model with higher-order interactions, allowing patients with progression-free survival (PFS) ≥12 months and patients with PFS <12 months to exhibit different longitudinal (linear) trajectories for each microbial feature. While we focus on the overall comparison between patients with PFS ≥12 and PFS <12 months averaging over the effect of multiple confounders, our methodology also allowed us to analyze microbial dynamics between patients with PFS ≥12 and PFS <12 months in three relevant clinical scenarios, namely therapy regimen (mono versus combination ICB), the development of ICB-induced colitis and concomitant proton-pump inhibitor (PPI) use. The latter two have well-studied effects on the gut microbiome^{19,20}.

Results

Cohort characteristics

Cohort characteristics are summarized in Table 1. We recruited 175 patients from five distinct cohorts across the Netherlands, the United Kingdom and Spain who were treated with ICB for unresectable stage 3 and stage 4 cutaneous melanoma, as previously described^{4–6,9–12}. A total of 117 (67%) patients received single agent treatment with an anti-programmed cell death (PD)-1 antibody (nivolumab or pembrolizumab), while 58 (33%) patients received combination therapy with anti-PD-1 and anti-cytotoxic T-lymphocyte-associated antigen (CTLA)-4 antibody (ipilimumab). We used the Response Evaluation Criteria in Solid Tumors (RECIST v.1.1) to determine tumor response (Methods). To capture patients who are alive or progression-free at late time points, we defined clinical endpoints as PFS at 12 months (PFS12) and overall survival (OS). PFS was defined as the time from the initial immunotherapy

to disease progression or death, comparing patients achieving a PFS of 12 months or longer and patients with a PFS of less than 12 months. PFS12 was reached by 83 (47%) participants, and the overall median OS was 34.1 months (minimum of 0.39 months, maximum of 93.4 months; censoring date, 28 March 2023). OS was defined for a subset of patients ($n = 147$ patients) as the time in months from initiation of treatment to occurrence of death from any cause. Patients were followed over a maximum period of 7.3 years (median of 4.3 years) after providing the first fecal sample. Fecal samples were collected at baseline and three subsequent treatment visits over a period of 12 weeks (Methods and Extended Data Fig. 1).

Taxonomic profiling was performed at the level of species-level genome bins (SGBs) using MetaPhlan4, which represent both existing and yet-to-be-characterized microbial species¹⁷. We first analyzed which SGBs' and MetaCyc pathways' relative abundances were differentially abundant between patients with PFS ≥12 and PFS <12 months averaging over the effect of confounders such as therapy regimen, development of ICB-induced colitis and other irAEs, concomitant use of PPIs, previous use of antibiotics, previous v-raf murine sarcoma viral oncogene homolog B1 (BRAF) or mitogen-activated protein kinase (MEK)-targeted therapy, and cancer center (Methods). Each regression parameter in our Bayesian model was represented by a marginal posterior probability distribution. We computed post hoc contrasts (see Supplementary Table 1 for the number of patient samples per contrast and study visit) for which we concluded that a microbial SGB or pathway is differentially abundant between cases and controls if 90% of its posterior distribution does not cover zero (that is, 90% Bayesian confidence level (BCL); other BCLs are reported in Supplementary Tables 2–12). At 90% BCL, we observed 62 (14.3%)

and 41 (9.4%) SGBs that exhibited increasing or decreasing slopes in patients with PFS ≥ 12 and PFS < 12 months, respectively (Supplementary Table 2), and 99 (22.8%) SGBs that were able to discriminate between patients with PFS ≥ 12 and PFS < 12 months in at least one study visit (90% BCL; range: 342 (50% BCL)–3 (100% BCL); Supplementary Table 3). Of these 99 SGBs, 20 were differentially abundant only at baseline, 42 were differentially abundant only after the start of ICB and 5 and 4 remained at consistently higher abundances in patients with PFS ≥ 12 and PFS < 12 months, respectively, at baseline and all subsequent study visits (Fig. 1a and Supplementary Table 4). To aid in the interpretation, Fig. 1a,b displays the longitudinal trajectories (that is, slopes) of two example SGBs and one MetaCyc pathway for patients with PFS ≥ 12 and PFS < 12 months, respectively. A clear example is *Sellimonas intestinalis* (SGB4617), which is not differentially abundant between patients with PFS ≥ 12 and PFS < 12 months at baseline (as illustrated by a gray cell at T0 in Fig. 1a). Beyond baseline, however, the expected abundance (represented in centered log ratio coordinates) increases sharply (as illustrated by a vivid red cell in Fig. 1a) in patients with PFS < 12 months while decreasing slightly (as illustrated by a light blue cell in Fig. 1a) in patients with PFS ≥ 12 months. Thus, the average difference between these two patient groups increases (in absolute terms) across the study visits (as illustrated by the increasingly darker brown shades from T1 towards T3 in Fig. 1a). The five SGBs that had consistently higher abundances in patients with PFS ≥ 12 months were *Agathobaculum butyriciproducens* (SGB14993 group), *Intestinibacter bartlettii* (SGB6140), *Dorea* sp. AF24 7LB (SGB4571), *Lactobacillus gasseri* (SGB7038 group) and *Lacrimispora celerecrescens* (SGB4868), whereof the latter two also exhibited increasing abundances (that is, positive slopes) over the study period (Fig. 1a and Supplementary Table 4). Three of these species have recently been associated with response in two new studies utilizing MetaPhlan4, one meta-analysis²¹ and one phase 1 FMT trial of ICB-naive patients²². These five species represent fiber degrading taxa capable of short chain fatty acid (SCFA) synthesis that has been linked to plant-based diets^{12,23,24}. Consequently, we also observed higher abundances of metabolic pathways (PWY-6396: superpathway of 2,3-butanediol biosynthesis; PWY-P124: *Bifidobacterium* shunt; PWY-6435: 4-hydroxybenzoate biosynthesis V; and PWY-5088: L-glutamate degradation VIII (to propanoate)) involved in the synthesis of SCFAs or their precursors in patients with PFS ≥ 12 months across multiple study visits (Fig. 1c and Supplementary Table 5), supporting a potential benefit of microbially produced SCFAs and an adjuvant role of fiber for ICB^{7,25}. Patients with PFS < 12 months, on the other hand, were enriched across all four study visits with *Ruthenibacterium lactatiformans* (SGB15271), *Prevotella copri* clade A (SGB1626), *Ruminococcaceae* unclassified (SGB15265 group) and an unidentified SGB from the phylum Bacteroidetes (SGB1957; Fig. 1a and Supplementary Table 4). In previous baseline studies, *P. copri* has been associated with ICB response^{26,27}. However, in the recent meta-analysis by Thomas et al.²¹, this particular SGB (SGB1626) was only associated with response in 5/12 cohorts and

with 3/9 different statistical methods. We found that patients with PFS < 12 months exhibited higher abundances of several pathways involved in menaquinol (vitamin K) synthesis at baseline and during early treatment (Fig. 1c and Supplementary Table 5). Menaquinol synthesis pathways are enriched in various chronic inflammatory and cardiovascular diseases^{28–31}. Fecal menaquinone levels have been correlated with the abundance of *Prevotella* and *Bacteroides* species and are susceptible to microbiome-targeted diets³², suggesting that menaquinol could represent an early marker of nonresponse that is amenable to dietary intervention. In contrast, patients achieving PFS12 exhibited higher abundances of a polyamine synthesis pathway (POLYAMINSYN3-PWY: superpathway of polyamine biosynthesis II) across the three study visits after baseline, but not at baseline. Polyamines are autophagy inducers³³ that are implicated in immune regulation and have been shown to improve anti-cancer immunity in mice, synergizing with anti-PD ligand 1 immunotherapy^{22,34}. Polyamines, including spermidine, are naturally occurring in foods and can be synthesized by the gut microbiome, suggesting a potential beneficial role for spermidine-enriched diets³⁵.

To assess whether the five and four SGBs that had consistently higher abundances in patients with PFS ≥ 12 and PFS < 12 months, respectively, could serve as a predictive marker for PFS12, we constructed a balance (a type of log ratio) between these SGBs and tested whether it could predict PFS12 in each study visit (Fig. 2a). We found that this balance could discriminate between patients with PFS ≥ 12 and PFS < 12 months in all but the last study visit (two-sided Wilcoxon test: $P_{T0} = 0.00085$, $P_{T1} = 0.0007$, $P_{T2} = 0.0005$ and $P_{T3} = 0.1$; Fig. 2b) with a moderate predictive ability across visits (area under the curve (AUC) from 100 times repeated five-fold cross-validation, measured as mean AUC \pm standard deviation (s.d.): AUC_{T0} 0.659 \pm 0.092, AUC_{T1} 0.666 \pm 0.091, AUC_{T2} 0.739 \pm 0.118 and AUC_{T3} 0.655 \pm 0.129; Fig. 2c). When we expanded this balance to include SGBs that were differentially abundant in all but the last study visit, its predictive ability increased across all study visits (AUC_{T0} 0.771 \pm 0.088, AUC_{T1} 0.706 \pm 0.094, AUC_{T2} 0.783 \pm 0.118 and AUC_{T3} 0.765 \pm 0.138; Extended Data Fig. 3a,b). Stratifying patients on the basis of whether they harbored higher or lower than median values of these two balances showed that patients above the median exhibited longer OS compared to patients below the median (first balance: OS_{High} of 35.4 versus OS_{Low} 28.4 months; hazard ratio (HR) of 1.669, $P = 0.035$; Fig. 2d; second balance: OS_{High} of 37.0 versus OS_{Low} of 26.9 months; HR of 1.792, $P = 0.014$; Extended Data Fig. 3c). Results did not quantitatively change when we substituted OS with continuous PFS (first balance: HR of 1.685, $P = 0.022$; second balance: HR = 2.25, $P = 0.0004$) and/or when we treated each balance as a continuous score (first balance: HR_{OS} = 0.828, $P_{OS} = 0.001$; second balance: HR_{OS} of 0.752, $P_{OS} = 0.0002$; Extended Data Fig. 4; first balance: HR_{PFS} of 0.829, $P_{PFS} = 0.0005$; second balance: HR_{PFS} of 0.727, $P_{PFS} = 8.93 \times 10^{-6}$).

We next tested the generalizability of the balance described in Fig. 2a by computing it for patients from six independent melanoma cohorts^{5,7–10,12}. Despite small sample sizes and large heterogeneity

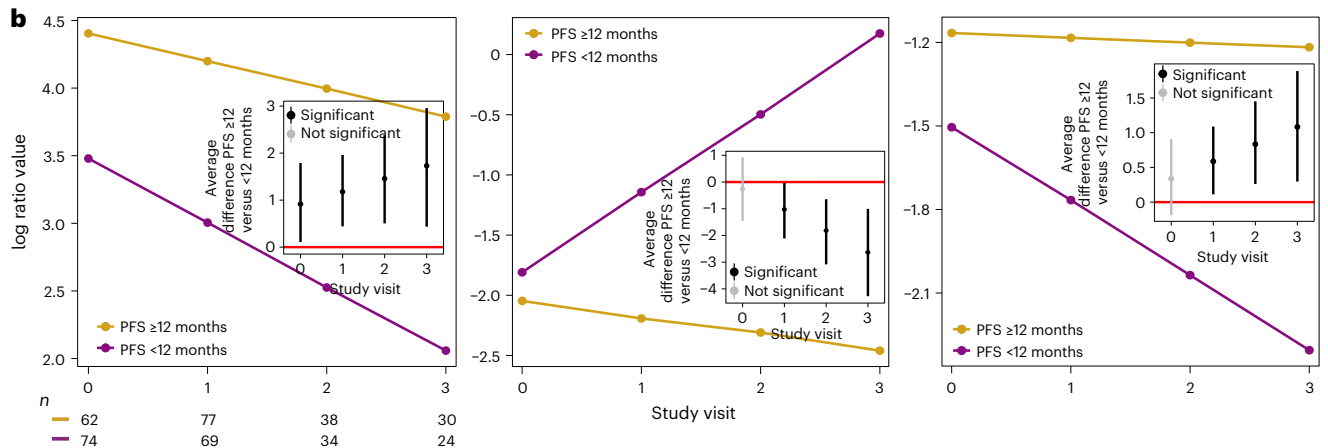
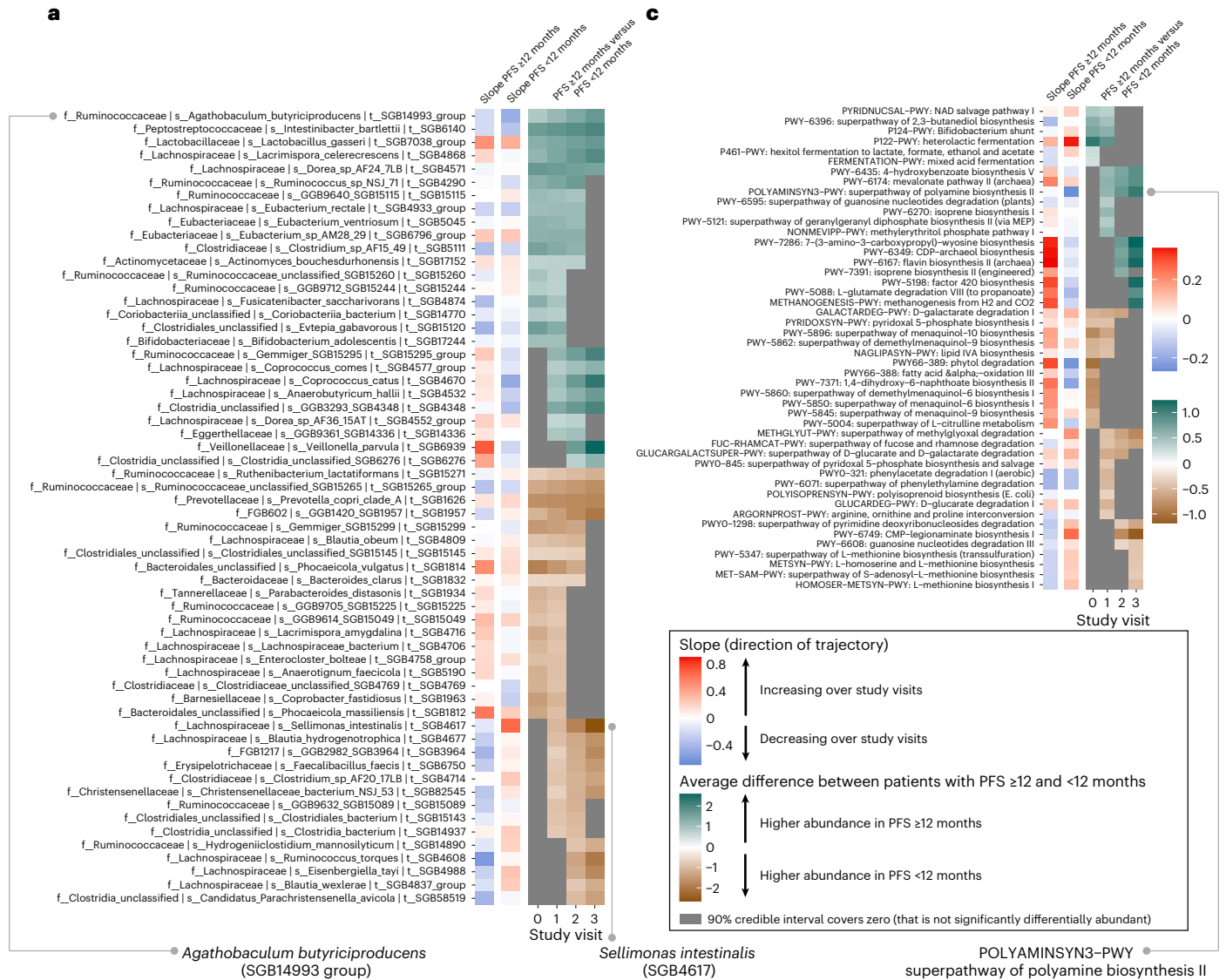
Fig. 1 | High-level view of gut microbiome dynamics in patients with PFS ≥ 12 and PFS < 12 months. a, For each microbial SGB listed, slopes are shown (that is, whether it is increasing or decreasing over study visits) in patients with PFS ≥ 12 ($n = 83$) and PFS < 12 months ($n = 92$), respectively. For increased readability, SGBs differentially abundant in only one study visit have been removed (see Extended Data Fig. 2 for all SGBs). Red and blue colors indicate whether the focal SGB is increasing or decreasing in its abundance over study visits, respectively, with the strength of the colors corresponding to the steepness of the slope, with darker shades indicating steeper increases/decreases. It then shows, in the teal–brown heatmap, the average difference between the two slopes (that is, between patients with PFS ≥ 12 and PFS < 12 months) across the different study visits. Non-gray cells in the heatmap correspond to the focal SGB's log fold change in abundance between patients with PFS ≥ 12 and PFS < 12 months, respectively. Teal cells correspond to study visits for which the abundance of the focal SGB

is higher in patients with PFS ≥ 12 than with PFS < 12 months, and vice versa for brown cells (at 90% BCL). Gray cells denote differences between patients with PFS ≥ 12 and PFS < 12 months whose 90% credible interval cover zero. **b**, Three example features and how they increase and/or decrease in their expected abundance (represented in centered log ratio coordinates) over the study visits in patients with PFS ≥ 12 months (yellow slope) and in patients with PFS < 12 months (purple slope). For each microbial SGB or pathway, the inset figure then displays the average difference between the two slopes at each study visit, including its 90% credible interval. These averages are the same as depicted in the teal–brown heatmap in **a**, and significance is deemed by evaluating whether or not the 90% credible interval covers zero. **c**, Microbial pathways are shown, similar to the format in **a**. The number (n) represents the number of patient samples at each visit for patients with PFS ≥ 12 and PFS < 12 months.

in terms of DNA isolation protocols and sequencing platforms (Supplementary Table 6), this analysis showed that the balance achieves a comparable AUC in several of the independent cohorts (Extended Data Fig. 5a,b). However, only in the cohort with a reasonably large number of patients ($N = 112$) did we find that the balance could discriminate between patients with PFS ≥ 12 and PFS < 12 months (two-sided Wilcoxon test, $P = 0.04$; Extended Data Fig. 5c). While limited in sample size ($N = 27$), the balance also

predicted OS in one of the independent cohorts ($P = 0.024$; Extended Data Fig. 5d).

Our analysis also revealed several SGBs only associated with PFS12 at baseline but not thereafter, many of which have not been previously reported in association with ICB, potentially owing to a lower resolution in taxonomic profiling (Extended Data Fig. 2 and Supplementary Table 4). For example, patients with PFS ≥ 12 months were enriched with *Romboutsia timonensis* (SGB6148), *Limosilactobacillus fermentum*



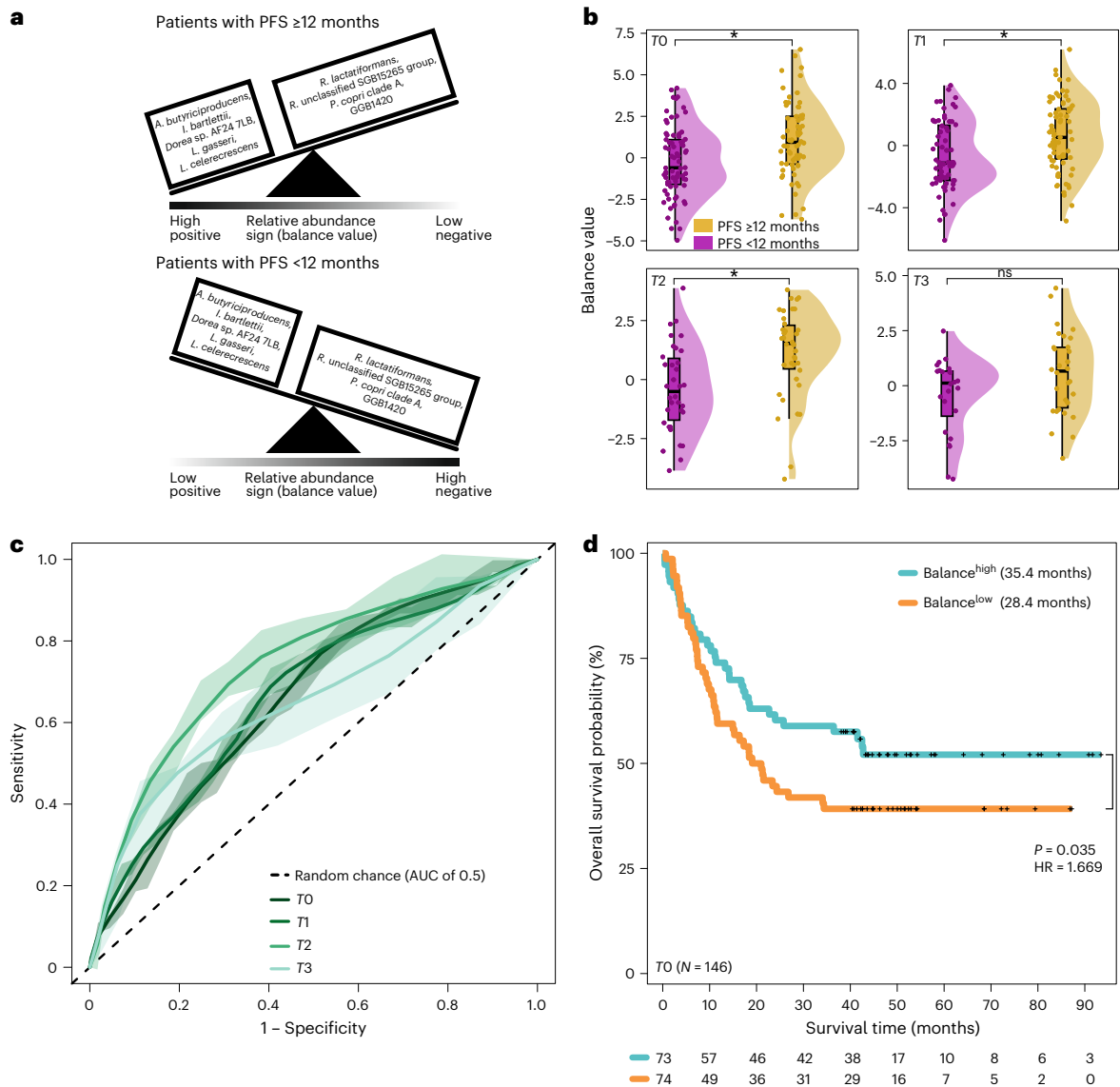


Fig. 2 | A longitudinal balance of microbial taxa (SGBs) predicts OS at baseline. **a**, Schematic illustration of a balance between the five SGBs that were consistently higher in patients with PFS ≥ 12 months (*A. butyrificiproducens* SGB14993 group, *I. bartlettii* SGB6140, *Dorea* sp. AF24 7LB SGB4571, *L. gasseri* SGB7038 group and *L. celerecrescens* SGB4868) and the four SGBs that were found to be consistently higher in patients with PFS < 12 months (*R. lactatiformans* SGB15271, *R. unclassified* SGB15265 group, *P. copri* clade A SGB1626 and an unidentified SGB from the phylum Bacteroidetes SGB1957). In patients with PFS ≥ 12 and PFS < 12 months, the balance is tilted to the left and right side, respectively. **b**, The balance's ability to discriminate between patients with PFS ≥ 12 ($n = 83, n_0 = 62, n_1 = 77, n_2 = 38$ and $n_3 = 30$) and PFS < 12 months ($n = 92, n_0 = 74, n_1 = 69, n_2 = 34$ and $n_3 = 24$) months across study visits (two-sided

Wilcoxon test: $P_{T_0} = 0.00085, P_{T_1} = 0.0007, P_{T_2} = 0.0005$ and $P_{T_3} = 0.1$). Boxplots represent minima, Q1, Q2, Q3 and maxima. **c**, The balance's predictive ability expressed as the AUC computed from 100 times repeated five-fold cross-validation. Each line shows, for each study visit, the average across the 100 times repeated five-fold cross-validations with the shaded area representing the 95% CI (mean AUC \pm s.d.: AUC_{T0} 0.659 \pm 0.092, AUC_{T1} 0.666 \pm 0.091, AUC_{T2} = 0.739 \pm 0.118 and AUC_{T3} 0.655 \pm 0.129). The dashed diagonal line represents random chance. **d**, Kaplan–Meier curves and multivariable Cox regression of OS in months for 146 patients at baseline according to high (above median; teal) and low (below median; orange) values of the balance after adjusting for age, sex, BMI, previous therapy, PPI and antibiotics use.

(SGB7106) and *Blautia schinkii* (SGB4825), while patients with PFS < 12 months had higher abundances of *Eubacterium siraeum* (SGB4198 group), *Oscillibacter* sp. ER4 (SGB15254) and *Dysosmobacter* sp. NSJ 60 (SGB15124) at baseline but not at subsequent study visits (Extended Data Fig. 2 and Supplementary Table 4). Stratifying patients on the basis of the median value of a balance between the 9 and 11 SGBs that, only at baseline, had higher abundances in patients with PFS ≥ 12 and PFS < 12 months, respectively, we could predict OS at baseline (OS_{High} of 35.5 months versus OS_{Low} of 28.4 months; HR of 1.639, $P = 0.034$; Extended Data Fig. 6).

Microbial associations that emerge after ICB initiation
While microbial taxa that are able to differentiate between patients with PFS ≥ 12 and PFS < 12 months at baseline may serve as important predictive and/or prognostic biomarkers, studying microbial taxa longitudinally could derive novel mechanistic insights in addition to becoming a new way to monitor ICB efficacy and irAEs. Therefore, we next identified SGBs that were only discriminative of patients with PFS ≥ 12 and PFS < 12 months after ICB initiation. We found higher abundances of several SCFA producers from the Lachnospiraceae family, which included *Coprococcus comes* (SGB4577 group), *Coprococcus*

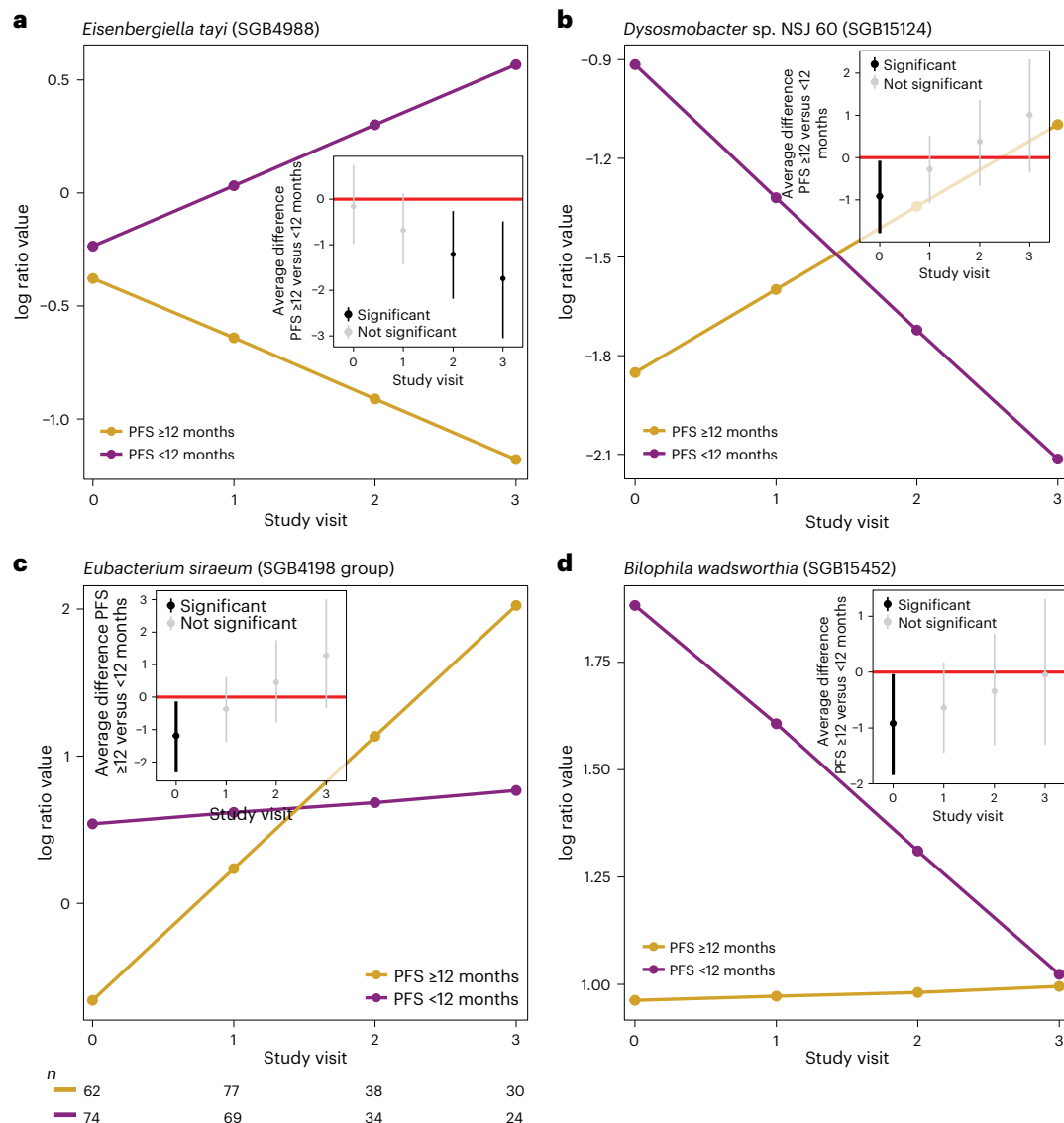


Fig. 3 | Different taxon dynamics in patients with PFS ≥ 12 and PFS <12 months. **a–d**, Four different dynamics exemplified by different microbial SGBs with different dynamics in patients with PFS ≥ 12 ($n_0 = 62$, $n_1 = 77$, $n_2 = 38$ and $n_3 = 30$) and PFS <12 ($n_0 = 74$, $n_1 = 69$, $n_2 = 34$ and $n_3 = 24$) months, where the slopes of patients with PFS ≥ 12 months (yellow slopes) and patients with PFS <12 months (purple slopes) diverge from similar baseline abundances (**a**, dynamics 2a, Extended Data Fig. 7a), where the slopes of patients with PFS ≥ 12 and PFS <12 months are crossing (**b**, generating opposite abundance patterns when comparing baseline to the last study visit, dynamics 3b, Extended Data Fig. 7b), where the slope of the patients with PFS <12 months is relatively unchanged

across the study visits compared to the slope of the patients with patients with PFS ≥ 12 months (**c**, dynamics 1c, Extended Data Fig. 7c); where the slope of the patients with PFS ≥ 12 months is relatively unchanged across the study visits compared to the slope of the patients with PFS <12 months (**d**, dynamics 2c, Extended Data Fig. 7c). The y axis shows the expected abundance (represented in centered log ratio coordinates) for each study visit (x axis). The corresponding inset figures show the average difference between patients with PFS ≥ 12 and PFS <12 months at each study visit, including its 90% credible interval. The number (n) represents the number of patient samples at each visit for patients with PFS ≥ 12 and PFS <12 months.

catus (SGB4670), *Gemmiger* (SGB15295 group) and *Anaerobutyricum hallii* (SGB4532) in patients with PFS ≥ 12 months after ICB initiation (Fig. 1a and Supplementary Table 4). These species have previously been associated with increased response and OS in patients treated with immunotherapy^{8,12,36,37}, but also with general health and a lower risk for metabolic and chronic inflammatory diseases²⁸. Patients with PFS <12 months, on the other hand, showed an increase in *Clostridium spiroforme* (SGB6747), several other Lachnospiraceae (*Blautia hydrogenotrophica* (SGB4677), *Blautia wexlerae* (SGB4837 group), *Ruminococcus torques* (SGB4608), *Sellimonas intestinalis* (SGB4617) and *Eisenbergiella tayi* (SGB4988) and Erysipelotrichaceae (*Turicibacter sanguinis* (SGB6847) and *Faecalibacillus faecis* (SGB6750)) species only after the start of ICB (Fig. 1a and Supplementary Table 4). Recent

studies have reported that *Eisenbergiella* sp., *B. wexlerae*, *C. spiroforme* and Erysipelotrichaceae were associated with resistance to ICB^{4,36} and enriched in patients with more aggressive tumors³⁸.

Abundance patterns in patients with PFS ≥ 12 and <12 months during ICB

Next, we took a closer look at specific abundance patterns in patients with PFS ≥ 12 and PFS <12 months over the study period. Here, we assess whether microbial abundances reversed, converged or diverged from baseline in patients with PFS ≥ 12 and PFS <12 months over the study period. We found that 22.8% (90% BCL; range: 74.7% (50% BCL)–0.7% (100% BCL)) of the SGBs increased or decreased after treatment initiation (Supplementary Table 3). Focusing on the aforementioned 99

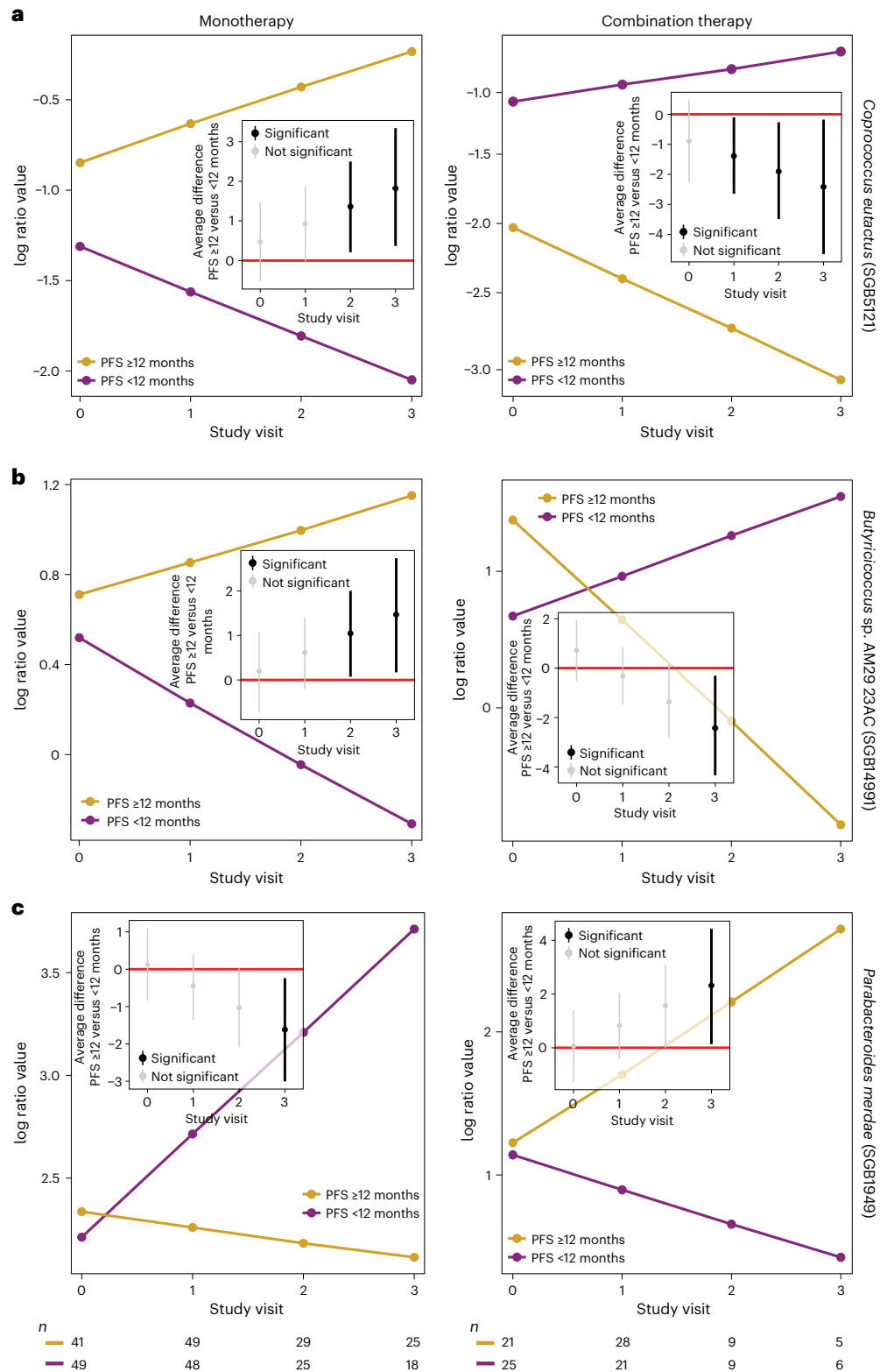


Fig. 4 | Divergent signals in monotherapy versus combination therapy.

a–c. Three examples out of the six SGBs that exhibited divergent patterns in monotherapy (PFS ≥ 12 : $n_0 = 41$, $n_1 = 49$, $n_2 = 29$ and $n_3 = 25$; PFS < 12 : $n_0 = 49$, $n_1 = 48$, $n_2 = 25$ and $n_3 = 18$) compared to combination therapy (PFS ≥ 12 : $n_0 = 21$, $n_1 = 28$, $n_2 = 9$ and $n_3 = 5$; PFS < 12 : $n_0 = 25$, $n_1 = 21$, $n_2 = 9$ and $n_3 = 6$): *C. eutactus* (SGB5121) (a), *Butyrivibrio* sp. AM29 23AC (SGB14991) (b) and *P. merdae* (SGB1949) (c). The y axis shows the expected abundance (represented in centered log ratio

coordinates) for each study visit (x axis). Left: anti-PD-1 monotherapy. Right: anti-PD-1/anti-CTLA-4 combination therapy. The corresponding inset figures show the average difference between patients with PFS ≥ 12 and PFS < 12 months at each study visit, including its 90% credible interval. The number (n) represents the number of patient samples at each visit for patients with PFS ≥ 12 and PFS < 12 months.

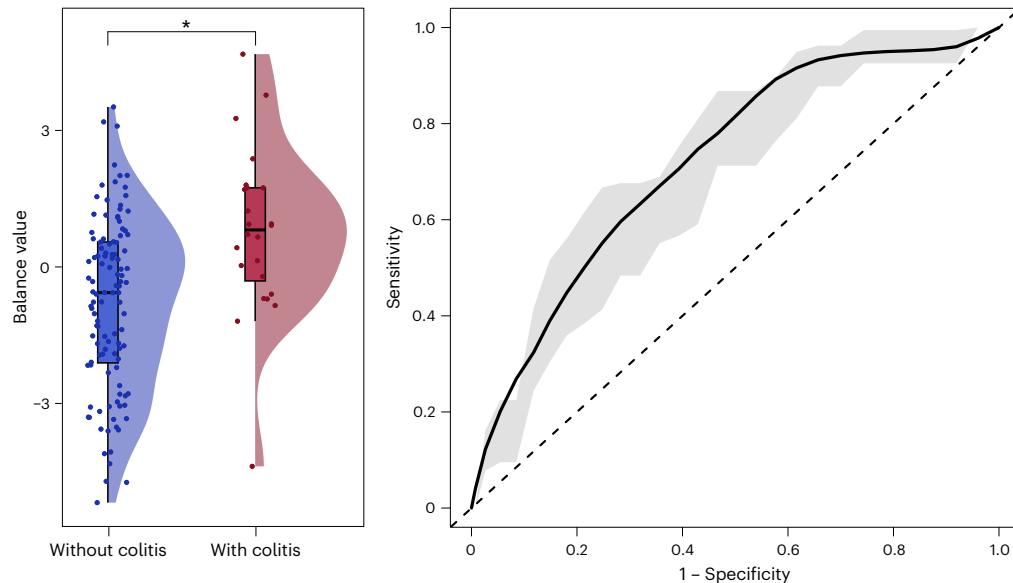


Fig. 5 | A balance predictive of ICB-induced colitis at baseline. A balance between the 10 SGBs associated with the presence of colitis (red; $n = 24$ patients) and the 12 SGBs associated with the absence of colitis (blue; $n = 112$ patients) at baseline is predictive of colitis development at baseline. Left: the balance's discriminatory ability (two-sided Wilcoxon test, $P_{70} = 0.00055$). Boxplots

represent minima, Q1, Q2, Q3 and maxima. Right: the same balance's predictive ability expressed as the averaged AUC computed from a 100 times repeated five-fold cross-validation (AUC mean \pm s.d. of 0.723 ± 0.121). The dashed diagonal line represents random chance.

SGBs that could discriminate between patients with PFS ≥ 12 and PFS < 12 months, we identified 22 SGBs for which patients with PFS ≥ 12 and PFS < 12 months exhibited intersecting slopes (Fig. 3b,c and Extended Data Fig. 7, dynamics 3ab). In these cases, patients with PFS ≥ 12 and PFS < 12 months had different initial abundances at baseline, with slopes crossing after the start of the treatment generating reverse abundance patterns at baseline compared to the last study visit. We found, for example, several SGBs that have been associated with various chronic and immune-mediated diseases, such as *Streptococcus thermophilus* (SGB8002) and *T. sanguinis* (SGB6847), which are dominant in the oral cavity, and *B. schinkii* (SGB4825), to exhibit opposite abundance patterns in patients with PFS ≥ 12 and PFS < 12 months at baseline compared to the last study visit with patients with PFS < 12 months and patients with PFS ≥ 12 months exhibiting positive and negative slopes, respectively. Other SGBs showed similar baseline abundances in patients with PFS ≥ 12 and PFS < 12 months to only diverge after the start of ICB (Fig. 3a and Extended Data Fig. 7, dynamics 1ab). For example, we found increasingly separating abundances of *Christensenellaceae bacterium* NSJ 53 (SGB82545), *E. tayi* (SGB4988; Fig. 3a), *Mediterraneibacter massiliensis* (SGB4595), *S. intestinalis* (SGB4617) and *Hydrogeniiclostridium mannosilyticum* (SGB14890) that increased in patients with PFS < 12 months and decreased in patients with PFS ≥ 12 months after the initiation of ICB (Extended Data Fig. 7, dynamics 2a and Supplementary Table 2).

Interestingly, we found 16 SGBs that remained relatively unchanged in patients with PFS < 12 months over the study period but showed larger changes in patients with PFS ≥ 12 months (Extended Data Fig. 7c, dynamics 1c). For example, only patients with PFS ≥ 12 months exhibited increasing abundances of *Lachnospiraceae bacterium* OF09 6 (SGB4966) and *Eubacterium siraeum* (SGB4198; Fig. 3c) and decreasing abundances of *F. faecis* (SGB6750) and *Fusicatenibacter saccharivorans* (SGB4874). Recent immunotherapy studies in renal cell carcinoma reported that *E. siraeum* was associated with improved survival and overall response rate^{8,12,36,37}, whereas *F. saccharivorans* and Erysipelotrichaceae members such as *F. faecis* were associated with resistance to ICB³⁹. Lastly, we found 14 SGBs, including *Bilophila wadsworthia* (SGB15452; Fig. 3d) and several *Clostridium* SGBs, which remained relatively unchanged in patients with PFS ≥ 12 months across all study visits while exhibiting larger changes in

patients with PFS < 12 months (Extended Data Fig. 7c, dynamics 2c). While these findings support previous studies showing that the gut microbiome can discriminate between response and nonresponse at baseline, they also suggest that ICB may induce different changes in the gut microbiome of patients with PFS ≥ 12 and PFS < 12 months, respectively. Thus, therapeutic targets that are based on baseline data only risk producing opposite or even unexpected effects.

The clinical context influences abundance patterns

Anti-PD-1 monotherapy versus anti-CTLA-4/anti-PD-1 combination therapy. We next analyzed microbial dynamics for different clinical scenarios and identified common and diverging signals of monotherapy (anti-PD-1) and combination therapy (anti-PD-1 and anti-CTLA-4). To avoid confounding by colitis and PPI use, which individually has considerable effects on the gut microbiome^{19,20}, we compared patients with PFS ≥ 12 months versus patients with PFS < 12 months on monotherapy (Extended Data Fig. 8 and Supplementary Table 7) or combination therapy (Extended Data Fig. 9 and Supplementary Table 8) who did not develop colitis and did not use PPIs, while also averaging over the effects of irAEs that were not colitis, previous antibiotics use, previous therapy and cancer center (Methods and Supplementary Information). We found 28 associations in common between monotherapy (27% of all associations at 90% BCL) and combination therapy (30% of all associations at 90% BCL), whereof 10 and 12 differentially abundant SGBs were shared between patients with PFS ≥ 12 and PFS < 12 months, respectively. Interestingly, the remaining six SGBs (of the 28 shared) exhibited opposite patterns in patients with PFS ≥ 12 versus patients with PFS < 12 months on monotherapy compared to combination therapy (Extended Data Figs. 8 and 9). These included *Coprococcus eutactus* (SGB5121), *Butyrivicoccus* sp. AM29 23AC (SGB14991) and *Parabacteroides merdae* (SGB1949), which had opposite slopes in patients with PFS ≥ 12 versus patients with PFS < 12 months on monotherapy compared to combination therapy (Fig. 4). Patients with PFS < 12 months treated with monotherapy showed increasing abundances of several *Bacteroides* species (except for *B. intestinalis*) across most or all study visits, which were not observed for combination therapy (Extended Data Figs. 8 and 9 and Supplementary Tables 7 and 8). These results confirm previous observations of

biphasic effects for the *Bacteroides* genus dependent on the specific treatment agent(s) used^{9,40,41}. SGBs that exhibited higher abundances in patients with PFS ≥ 12 months compared to patients with PFS < 12 months, regardless of therapy regimen, included *Lactocaseibacillus rhamnosus* (SGB7144), an unknown Firmicutes (SGB47850), three members from Lachnospiraceae (*Dorea* sp. AF24 7LB (SGB4571), *Dorea formicigenerans* (SGB4575), as reported previously⁴², and *C. comes* (SGB4577 group)) and four unidentified species from the family Ruminococcaceae (*Ruminococcaceae bacterium* (SGB15356), GGB9705 (SGB15224), GGB9712 (SGB15244) and GGB9677 (SGB15180); Extended Data Figs. 8 and 9 and Supplementary Tables 7 and 8).

ICB-induced colitis. We then aimed to identify SGBs associated with development or no development of colitis, averaging over the effects of all other predictors in our model, including PFS12 and therapy regimen (Extended Data Fig. 10 and Supplementary Table 9). We were particularly interested in colitis given the role of the gut microbiome in maintaining colonic immune homeostasis. Colitis was defined using the Common Terminology Criteria for Adverse Events (CTCAE) version 5, excluding intestinal symptoms of non-immune etiology. We found that butyrate producers, such as *Roseburia inulinivorans* (SGB4940) and *Roseburia hominis* (SGB4936), *A. butyriciproducens* (SGB14993 group), *Eubacterium rectale* (SGB4933 group), *Bacteroides thetaiotaomicron* (SGB1861) and two *Faecalibacterium prausnitzii* subspecies (SGB15342 and SGB15317) had higher abundances in patients who did not develop colitis after the start of ICB (Extended Data Fig. 10 and Supplementary Table 9). While all of these SGBs, apart from *R. inulinivorans* (SGB4940), exhibited negative slopes in both patients affected and patients unaffected by colitis, the decrease was larger in patients who developed colitis. It has been suggested that butyrate may be protective against ICB-induced colitis⁴²; thus a further reduction in the abundance of butyrate producing bacteria during ICB may predispose patients with already lower baseline abundances to colitis. We found that the patient group who did not develop ICB-induced colitis exhibited a higher abundance of *F. saccharivorans* (SGB4874), which has been shown to induce anti-inflammatory effects in ulcerative colitis⁴³ but has also been associated with resistance to ICB³⁹. While *Akkermansia muciniphila* has been associated with response in several baseline studies^{4,11}, we found that *A. muciniphila* (SGB9226) had higher baseline abundances in patients who developed colitis but decreased sharply in abundance thereafter (Extended Data Fig. 10 and Supplementary Table 9). In comparison, the group who did not develop colitis exhibited lower but somewhat increasing abundances of the same SGB (Extended Data Fig. 10 and Supplementary Table 9). While in our cohorts only this particular SGB was identified, there are four different *A. muciniphila* SGBs in the new MetaPhlan4 database. Finally, monitoring microbial taxa that are associated with colitis is an important first step toward developing strategies to ameliorate its effects. As a proof of concept, we tested whether a balance between the SGBs associated with development of colitis and the SGBs associated with no development of colitis at baseline (that is, at T0 in Extended Data Fig. 10) could predict colitis development at baseline. We found that this balance could discriminate between the two groups (two-sided Wilcoxon test, $P_{T0} = 0.00055$) with an acceptable predictive ability (AUC mean \pm s.d. of 0.723 ± 0.121 ; Fig. 5).

In our dataset, we found a relationship between PFS12 and irAEs that were not colitis (Fisher's exact test: $P = 0.002$; Supplementary Fig. 1). Compared to patients who achieved a PFS ≥ 12 months and developed colitis, we found that patients who achieved PFS ≥ 12 months but did not develop colitis exhibited higher abundances of four SGBs across the entire study period (*Blautia* sp. AF19 10LB (SGB4810), *Lachnospiraceae bacterium* (SGB4706), *Gordonibacter pamelaee* (SGB14807) and *Clostridium* sp. AF20 17LB (SGB4714); Supplementary Fig. 2 and Supplementary Table 10). On the other hand, we found seven SGBs that exhibited higher abundances, throughout

the study period, in patients with PFS ≥ 12 months who developed colitis, including several unclassified Clostridia species (Supplementary Fig. 2 and Supplementary Table 10). Interestingly, while patients with PFS ≥ 12 months without colitis showed enrichment in several *F. prausnitzii* SGBs (SGB15317, SGB15318 group, and SGB15342), *A. butyriciproducens* (SGB14993 group) and *R. hominis* (SGB4936), the abundance of *A. muciniphila* (SGB9226) was higher (but decreasing) in patients with PFS ≥ 12 months who developed colitis (Supplementary Fig. 2 and Supplementary Table 10). *F. prausnitzii* has previously been associated with the absence of colitis³⁷; hence our findings further support approaches targeting different subspecies of *F. prausnitzii* to counteract colitis while maintaining ICB efficacy.

While we found a difference in the proportion of patients who develop colitis on monotherapy (0.128) compared to combination therapy (0.310) (two-sided test of equal proportions: $\Delta = 0.182$; 95% CI: 0.036, 0.329; $\chi^2 = 7.259$; $P = 0.007$), we did not find a difference in the proportion of patients with PFS ≥ 12 months who developed colitis on monotherapy (0.051) compared to combination therapy (0.138) (two-sided test of equal proportions: $\Delta = 0.087$; 95% CI: -0.024, 0.197; $\chi^2 = 2.866$; $P = 0.09$). When we compared colitis development under combination versus monotherapy, we observed higher and increasing abundances of SGBs belonging to the *Streptococcus*, *Veillonella*, *Bacteroides* and *Eggerthella* genera, an overall signature resembling the gut microbiome of patients with inflammatory bowel disease²⁰ (Supplementary Fig. 3 and Supplementary Table 11).

PPI use. Finally, we investigated the effect of PPI use on patients with PFS ≥ 12 and PFS < 12 months (Supplementary Fig. 4 and Supplementary Table 12). To avoid confounding by combination therapy and colitis, we focused on the group of patients who were treated with monotherapy and did not develop ICB-induced colitis. Here we found that PPI users on monotherapy shared 33 associations with nonusers on monotherapy (at 90% BCL; Supplementary Table 13). For a few SGBs, patients with PFS ≥ 12 months exhibited different slopes for users and nonusers. For example, *S. thermophilus* (SGB8002) exhibited increasing abundances in nonusers with PFS ≥ 12 months and decreasing abundances in users with PFS ≥ 12 months. Similarly, *C. bacterium* NSJ 53 (SGB82545) and *B. caccae* (SGB1877) exhibited increasing and decreasing abundances in nonusers and users, respectively, with PFS < 12 months. While the Christensenellaceae family has been associated with health, *B. caccae*, *B. stercoris* and *P. vulgatus* have been linked to diseases such as inflammatory bowel disease and colorectal cancer^{44,45}.

Discussion

In this study, we longitudinally profiled the gut microbiome in a multi-center cohort of 175 patients with advanced melanoma undergoing ICB. Through Bayesian regression models with higher-order interactions, we characterized microbiome changes in patients with PFS ≥ 12 or PFS < 12 months during ICB, including in different clinical contexts such as therapy regimen, development of colitis and PPI use.

Previous studies conducted at baseline have led to an accumulating interest in SCFA producers as targets for increasing ICB efficacy, whereas species predictive of resistance to ICB have been associated with chronic immune-mediated or metabolic diseases⁴⁶. However, longitudinal studies of the gut microbiome dynamics during treatment with ICB have been lacking. We show that, during ICB, a number of SGBs have contrasting dynamics to what would be expected from baseline and that the same SGB can exhibit different trajectories depending on the clinical context. While the abundance of SCFA producers remained at a higher abundance or even increased in patients with PFS ≥ 12 months during treatment, the abundance of SGBs considered 'immunogenic' exhibited larger changes from baseline, with different dynamics in different clinical contexts. Patients with PFS < 12 months showed higher or increasing abundances of taxa that have

been associated with inflammatory diseases, such as *B. clarus*, *S. intestinalis* and *E. taylori*. However, when considering different clinical contexts, we also found several taxa regarded as ‘proinflammatory’ (for example, *P. merdae*, *Desulfovibrio piger* and *Streptococcus oralis*) to be enriched in patients with PFS \geq 12 months (Supplementary Fig. 5).

Comparing our results to two recent studies employing MetaPhlan4, we found many common SGBs associated with ICB response at baseline, including several SGBs that also were differentially abundant during therapy and in different clinical contexts in our study. For example, Thomas et al.²¹ found that *Eubacterium* sp. AM2829 (SGB6796 group) was associated with response in nine melanoma cohorts, four of which were not included in our study^{5,9,11,36}. The same SGB was enriched in responders 1 month after FMT²². In our study, it was associated with PFS \geq 12 months at baseline through to the second study visit, and at baseline in patients with PFS \geq 12 months on combination therapy. Another SGB, *L. celerecrecens* (SGB4868), which is part of the balance described in Fig. 2a, was associated with response in six melanoma cohorts, five of which were not included in our study^{9,11,12,36,47} analyzed by ref. 21 and also enriched in all responders one month after FMT²². The replicability of our results, both the main balance and specific SGBs, shows the robustness of our longitudinal analysis (Supplementary Tables 14 and 15).

Our findings provide an important roadmap for designing and interpreting microbiome-based intervention studies. Owing to the distinct longitudinal dynamics observed in this study, therapeutic targets developed only from baseline findings may produce opposite or unexpected results. This can further vary depending on the clinical context. While we confirm a higher or increasing abundance of several species that are currently being studied as consortia therapies, including *A. butyriciproducens*, *A. hallii*, *C. catus*, *E. rectale*, *Bifidobacterium adolescentis*, *F. prausnitzii*⁴⁸ and *B. thetaiotaomicron*⁴⁹, other members of these consortia showed an increase in patients with PFS <12 months in our study, such as *R. torques*, *Parabacteroides distasonis*⁴⁸ and *B. clarus*⁴⁹, or had opposite trajectories depending on the therapy regimen (for example, increase of several *Bacteroides* SGBs and *P. merdae* in patients with PFS <12 months on anti-PD-1 monotherapy)⁴⁸.

Our results could also be used to disentangle the effect of FMT from the longitudinal effect of ICB and important confounders on the gut microbiome. Recent phase I clinical trials suggest that FMT from responders^{50,51} or healthy donors²² combined with anti-PD-1 can induce response in a subset of ICB-refractory (OR 20–30% in refs. 50,51) and ICB-naïve patients (OR 65% in ref. 22). Without performing FMTs, we observe similar taxa changes in patients with PFS \geq 12 months (Supplementary Tables 14 and 15), suggesting that FMT synergizes with ICB to improve responses. Inter-individual variability in the response and engraftment of strains is widely described after FMT for different clinical contexts^{52,53} in which various treatment and host factors play a role^{16,22,54,55}. We observed different dynamics of the shared SGBs depending on the clinical context (Supplementary Tables 14 and 15), findings that could be used to help optimize donor-recipient stratification in future trials.

To conclude, this study underlines the dynamic nature of the gut microbiome and indicates that longitudinal profiling at finer taxonomic resolution in association with host factors is critical for guiding microbiome-targeted interventions aimed at improving treatment outcomes. Limitations of this study include (but are not restricted to) simplifying microbial dynamics to linear trajectories, comparability with previous studies using different taxonomic databases and a smaller number of patient samples for some of the post hoc comparisons, which limits the generalizability of some of our results. To further validate our findings and move the clinical gut microbiome field forward from a biomarker perspective to actionable treatments, continued efforts should go into longitudinal profiling of ICB patients at larger scales, linking the gut microbiome, metabolome and immune to treatment outcome.

Online content

Any methods, additional references, Nature Portfolio reporting summaries, source data, extended data, supplementary information, acknowledgements, peer review information; details of author contributions and competing interests; and statements of data and code availability are available at <https://doi.org/10.1038/s41591-024-02803-3>.

References

- Ribas, A. & Wolchok, J. D. Cancer immunotherapy using checkpoint blockade. *Science* **359**, 1350–1355 (2018).
- Hammers, H. J. et al. Safety and efficacy of nivolumab in combination with ipilimumab in metastatic renal cell carcinoma: the CheckMate 016 study. *J. Clin. Oncol.* **35**, 3851–3858 (2017).
- Sznol, M. et al. Pooled analysis safety profile of nivolumab and ipilimumab combination therapy in patients with advanced melanoma. *J. Clin. Oncol.* **35**, 3815–3822 (2017).
- Lee, K. A. et al. Cross-cohort gut microbiome associations with immune checkpoint inhibitor response in advanced melanoma. *Nat. Med.* **28**, 535–544 (2022).
- McCulloch, J. A. et al. Intestinal microbiota signatures of clinical response and immune-related adverse events in melanoma patients treated with anti-PD-1. *Nat. Med.* **28**, 545–556 (2022).
- Simpson, R. C. et al. Diet-driven microbial ecology underpins associations between cancer immunotherapy outcomes and the gut microbiome. *Nat. Med.* **28**, 2344–2352 (2022).
- Spencer, C. N. et al. Dietary fiber and probiotics influence the gut microbiome and melanoma immunotherapy response. *Science* **374**, 1632–1640 (2021).
- Peters, B. A. et al. Relating the gut metagenome and metatranscriptome to immunotherapy responses in melanoma patients. *Genome Med.* **11**, 61 (2019).
- Gopalakrishnan, V. et al. Gut microbiome modulates response to anti-PD-1 immunotherapy in melanoma patients. *Science* **359**, 97–103 (2018).
- Matson, V. et al. The commensal microbiome is associated with anti-PD-1 efficacy in metastatic melanoma patients. *Science* **359**, 104–108 (2018).
- Routy, B. et al. Gut microbiome influences efficacy of PD-1-based immunotherapy against epithelial tumors. *Science* **359**, 91–97 (2018).
- Frankel, A. E. et al. Metagenomic shotgun sequencing and unbiased metabolomic profiling identify specific human gut microbiota and metabolites associated with immune checkpoint therapy efficacy in melanoma patients. *Neoplasia* **19**, 848–855 (2017).
- Olsson, L. M. et al. Dynamics of the normal gut microbiota: a longitudinal one-year population study in Sweden. *Cell Host Microbe* **30**, 726–739.e3 (2022).
- Chen, L. et al. The long-term genetic stability and individual specificity of the human gut microbiome. *Cell* **184**, 2302–2315.e12 (2021).
- Franzosa, E. A. et al. Identifying personal microbiomes using metagenomic codes. *Proc. Natl Acad. Sci. USA* **112**, E2930–E2938 (2015).
- Lavelle, A. & Sokol, H. Understanding and predicting the efficacy of FMT. *Nat. Med.* **28**, 1759–1760 (2022).
- Blanco-Míguez, A. et al. Extending and improving metagenomic taxonomic profiling with uncharacterized species using MetaPhlan 4. *Nat. Biotechnol.* <https://doi.org/10.1038/s41587-023-01688-w> (2023).
- Caspi, R. et al. The MetaCyc database of metabolic pathways and enzymes and the BioCyc collection of pathway/genome databases. *Nucleic Acids Res.* **42**, D459–D471 (2014).
- Halfvarson, J. et al. Dynamics of the human gut microbiome in inflammatory bowel disease. *Nat. Microbiol.* **2**, 17004 (2017).

20. Imhann, F. et al. Proton pump inhibitors affect the gut microbiome. *Gut* **65**, 740–748 (2016).
21. Thomas, A. M. et al. Gut OncoMicrobiome Signatures (GOMS) as next-generation biomarkers for cancer immunotherapy. *Nat. Rev. Clin. Oncol.* **20**, 583–603 (2023).
22. Routy, B. et al. Fecal microbiota transplantation plus anti-PD-1 immunotherapy in advanced melanoma: a phase I trial. *Nat. Med.* **29**, 2121–2132 (2023).
23. Asnicar, F. et al. Microbiome connections with host metabolism and habitual diet from 1,098 deeply phenotyped individuals. *Nat. Med.* **27**, 321–332 (2021).
24. Morrison, D. J. & Preston, T. Formation of short chain fatty acids by the gut microbiota and their impact on human metabolism. *Gut Microbes* **7**, 189–200 (2016).
25. Nomura, M. et al. Association of short-chain fatty acids in the gut microbiome with clinical response to treatment with nivolumab or pembrolizumab in patients with solid cancer tumors. *JAMA Netw. Open* **3**, e202895 (2020).
26. Pietrzak, B. et al. A clinical outcome of the Anti-PD-1 therapy of melanoma in polish patients is mediated by population-specific gut microbiome composition. *Cancers* **14**, 5369 (2022).
27. Jin, Y. et al. The diversity of gut microbiome is associated with favorable responses to anti-programmed death 1 immunotherapy in Chinese patients with NSCLC. *J. Thorac. Oncol.* **14**, 1378–1389 (2019).
28. Gacesa, R. et al. Environmental factors shaping the gut microbiome in a Dutch population. *Nature* **604**, 732–739 (2022).
29. Vich Vila, A. et al. Gut microbiota composition and functional changes in inflammatory bowel disease and irritable bowel syndrome. *Sci. Transl. Med.* **10**, eaap8914 (2018).
30. Dash, N. R. & Al Bataineh, M. T. Metagenomic analysis of the gut microbiome reveals enrichment of menaquinones (vitamin K2) pathway in diabetes mellitus. *Diabetes Metab. J.* **45**, 77–85 (2021).
31. Kurilshikov, A. et al. Gut microbial associations to plasma metabolites linked to cardiovascular phenotypes and risk. *Circ. Res.* <https://doi.org/10.1161/circresaha.118.314642> (2019).
32. Karl, J. P. et al. Fecal menaquinone profiles of overweight adults are associated with gut microbiota composition during a gut microbiota-targeted dietary intervention. *Am. J. Clin. Nutr.* **102**, 84–93 (2015).
33. Madeo, F., Eisenberg, T., Pietrocola, F. & Kroemer, G. Spermidine in health and disease. *Science* **359**, eaan2788 (2018).
34. Lévesque, S. et al. A synergistic triad of chemotherapy, immune checkpoint inhibitors, and caloric restriction mimetics eradicates tumors in mice. *Oncoimmunology* **8**, e1657375 (2019).
35. Montégut, L., de Cabo, R., Zitvogel, L. & Kroemer, G. Science-driven nutritional interventions for the prevention and treatment of cancer. *Cancer Discov.* **12**, 2258–2279 (2022).
36. Derosa, L. et al. Gut bacteria composition drives primary resistance to cancer immunotherapy in renal cell carcinoma patients. *Eur. Urol.* **78**, 195–206 (2020).
37. Chaput, N. et al. Baseline gut microbiota predicts clinical response and colitis in metastatic melanoma patients treated with ipilimumab. *Ann. Oncol.* **28**, 1368–1379 (2017).
38. Terrisse, S. et al. Intestinal microbiota influences clinical outcome and side effects of early breast cancer treatment. *Cell Death Differ.* **28**, 2778–2796 (2021).
39. Salgia, N. J. et al. Stool microbiome profiling of patients with metastatic renal cell carcinoma receiving anti-PD-1 immune checkpoint inhibitors. *Eur. Urol.* **78**, 498–502 (2020).
40. Roy, S. & Trinchieri, G. Microbiota: a key orchestrator of cancer therapy. *Nat. Rev. Cancer* **17**, 271–285 (2017).
41. Vétizou, M. et al. Anticancer immunotherapy by CTLA-4 blockade relies on the gut microbiota. *Science* **350**, 1079–1084 (2015).
42. Chang, A. E. et al. Targeting the gut microbiome to mitigate immunotherapy-induced colitis in cancer. *Trends Cancer Res.* **7**, 583–593 (2021).
43. Takeshita, K. et al. A single species of clostridium subcluster XIVa decreased in ulcerative colitis patients. *Inflamm. Bowel Dis.* **22**, 2802–2810 (2016).
44. Read, E., Curtis, M. A. & Neves, J. F. The role of oral bacteria in inflammatory bowel disease. *Nat. Rev. Gastroenterol. Hepatol.* **18**, 731–742 (2021).
45. Thomas, A. M. et al. Metagenomic analysis of colorectal cancer datasets identifies cross-cohort microbial diagnostic signatures and a link with choline degradation. *Nat. Med.* **25**, 667–678 (2019).
46. Derosa, L. et al. Microbiota-centered interventions: the next breakthrough in immuno-oncology? *Cancer Discov.* **11**, 2396–2412 (2021).
47. Derosa, L. et al. Intestinal Akkermansia muciniphila predicts clinical response to PD-1 blockade in patients with advanced non-small-cell lung cancer. *Nat. Med.* **28**, 315–324 (2022).
48. Spreafico, A. et al. First-in-class Microbial Ecosystem Therapeutic 4 (MET4) in combination with immune checkpoint inhibitors in patients with advanced solid tumors (MET4-IO trial). *Ann. Oncol.* **34**, 520–530 (2023).
49. Tanoue, T. et al. A defined commensal consortium elicits CD8 T cells and anti-cancer immunity. *Nature* **565**, 600–605 (2019).
50. Baruch, E. N. et al. Fecal microbiota transplant promotes response in immunotherapy-refractory melanoma patients. *Science* **371**, 602–609 (2021).
51. Davar, D. et al. Fecal microbiota transplant overcomes resistance to anti-PD-1 therapy in melanoma patients. *Science* **371**, 595–602 (2021).
52. Ianiro, G. et al. Variability of strain engraftment and predictability of microbiome composition after fecal microbiota transplantation across different diseases. *Nat. Med.* **28**, 1913–1923 (2022).
53. Schmidt, T. S. B. et al. Drivers and determinants of strain dynamics following fecal microbiota transplantation. *Nat. Med.* **28**, 1902–1912 (2022).
54. Halsey, T. M. et al. Microbiome alteration via fecal microbiota transplantation is effective for refractory immune checkpoint inhibitor-induced colitis. *Sci. Transl. Med.* **15**, eabq4006 (2023).
55. Baruch, E. N., Gaglani, T. & Wargo, J. A. Fecal microbiota transplantation as a mean of overcoming immunotherapy resistant cancers – hype or hope?. *Ther. Adv. Med. Oncol.* **13**, 17588359211045853 (2021).

Publisher's note Springer Nature remains neutral with regard to jurisdictional claims in published maps and institutional affiliations.

Open Access This article is licensed under a Creative Commons Attribution 4.0 International License, which permits use, sharing, adaptation, distribution and reproduction in any medium or format, as long as you give appropriate credit to the original author(s) and the source, provide a link to the Creative Commons license, and indicate if changes were made. The images or other third party material in this article are included in the article's Creative Commons license, unless indicated otherwise in a credit line to the material. If material is not included in the article's Creative Commons license and your intended use is not permitted by statutory regulation or exceeds the permitted use, you will need to obtain permission directly from the copyright holder. To view a copy of this license, visit <http://creativecommons.org/licenses/by/4.0/>.

© The Author(s) 2024

Johannes R. Björk ^{1,21}✉, Laura A. Bolte ^{1,21}, Andrew Maltez Thomas ², Karla A. Lee³, Niccolo Rossi³, Thijs T. Wind⁴, Lotte M. Smit⁴, Federica Armanini², Francesco Asnicar ², Aitor Blanco-Miguez ², Ruth Board⁵, Neus Calbet-Llopart^{6,7}, Lisa Derosa ⁸, Nathalie Dhomen ⁹, Kelly Brooks⁹, Mark Harland¹⁰, Mark Harries^{11,12}, Paul Lorigan^{13,14}, Paolo Manghi², Richard Marais¹⁵, Julia Newton-Bishop¹⁰, Luigi Nezi ¹⁶, Federica Pinto ², Miriam Potrony^{7,12}, Susana Puig ^{6,7}, Patricio Serra-Bellver¹³, Heather M. Shaw¹⁷, Sabrina Tamburini¹⁶, Sara Valpione^{9,13}, Levi Waldron ^{2,18}, Laurence Zitvogel ⁸, Moreno Zolfo², Elisabeth G. E. de Vries ⁴, Paul Nathan^{12,17}, Rudolf S. N. Fehrmann ⁴, Tim D. Spector³, Véronique Bataille^{3,19,20}, Nicola Segata^{2,16}, Geke A. P. Hospers ⁴ & Rinse K. Weersma ¹✉

¹Department of Gastroenterology and Hepatology, University of Groningen and University Medical Center Groningen, Groningen, the Netherlands.

²Department of CellularComputational and Integrative Biology, University of Trento, Trento, Italy. ³Department of Twin Research and Genetic Epidemiology, King's College London, London, UK. ⁴Department of Medical Oncology, Groningen University of Groningen and University Medical Center Groningen, Groningen, the Netherlands. ⁵Department of Oncology, Lancashire Teaching Hospitals NHS Trust, Preston, UK. ⁶Department of Dermatology, Melanoma Group, Hospital Clínic Barcelona, IDIBAPS, Universitat de Barcelona, Barcelona, Spain. ⁷Centro de Investigación Biomédica en Red en Enfermedades Raras, Instituto de Salud Carlos III, Barcelona, Spain. ⁸Gustave Roussy Cancer Center, U1015 INSERM and Oncobiome Network, University Paris Saclay, Villejuif-Grand-Paris, France. ⁹Division of Immunology, Immunity to Infection and Respiratory Medicine, University of Manchester, Manchester, UK. ¹⁰Division of Haematology and Immunology, Institute of Medical Research at St. James's, University of Leeds, Leeds, UK. ¹¹Department of Medical Oncology, Guys Cancer Centre, Guy's and St Thomas' NHS Trust, London, UK. ¹²Biochemical and Molecular Genetics Department, Hospital Clínic de Barcelona and IDIBAPS, University of Barcelona, Barcelona, Spain. ¹³The Christie NHS Foundation Trust, Manchester, UK. ¹⁴Division of Cancer Sciences, University of Manchester, Manchester, UK. ¹⁵Molecular Oncology Group, Cancer Research UK Manchester Institute, University of Manchester, Manchester, UK. ¹⁶European Institute of Oncology (Istituto Europeo di Oncologia), Milan, Italy. ¹⁷Department of Medical Oncology, Mount Vernon Cancer Centre, East and North Herts NHS Trust, Northwood, UK. ¹⁸Graduate School of Public Health and Health Policy, City University of New York, New York, NY, USA. ¹⁹Department of Dermatology, Mount Vernon Cancer Centre, Northwood, UK. ²⁰Department of Dermatology, Hemel Hempstead Hospital, West Hertfordshire NHS Trust, Hemel Hempstead, UK. ²¹These authors contributed equally: Johannes R. Björk, Laura A. Bolte.

✉e-mail: bjork.johannes@gmail.com; r.k.weersma@umcg.nl

Methods

Study design and cohort description

The prospective PRIMM cohorts. We prospectively recruited 128 patients with advanced melanoma who were treated with ICB between August 2015 and January 2020 in the UK studies Predicting Response to Immunotherapy for Melanoma with Gut Microbiome and Metabolomics (PRIMM-UK, $n = 54$) and the Netherlands studies (PRIMM-NL, $n = 74$, made up of eligible patients from the COLIPI, POINTING and OncoLifeS studies). PRIMM-UK (NCT03643289) is sponsored by East and North Hertfordshire NHS Trust with ethical approval from King's College London. OncoLifeS (METc number 2010/109), COLIPI (METc number 2012/085, NCT02600143) and POINTING (METc number 2018/350, NCT04193956) have all been approved by the Medical Ethical Committee (in Dutch: Medisch Ethische Toetsingscommissie or METc) of the University Medical Center Groningen in the Netherlands. OncoLifeS information is available on the Netherlands Trial Register⁵⁶. Fecal samples were collected from these patients before initiation of ICB and longitudinally at up to four treatment (study) visits: at baseline and before each subsequent treatment cycle over a period of 12 weeks (Supplementary Fig. 1). The time between two samples was 3 or 4 weeks, depending on the treatment regimen, with ipilimumab/nivolumab combination therapy and pembrolizumab monotherapy administered three times weekly and nivolumab monotherapy administered four times weekly. Written informed consent was obtained from all patients.

Other enrolled cohorts. Patients within the PRIMM cohorts were recruited in parallel, using aligned protocols⁴. Additional patients, treated between March 2015 and November 2019, were enrolled from cohorts outside the setting of the PRIMM study: Leeds ($n = 19$), Barcelona ($n = 11$) and Manchester ($n = 17$). Fecal samples were collected at time points similar to those used in our included prospective studies. Patient samples within the Manchester cohort were collected with written full-informed patient consent under Manchester Cancer Research Centre Biobank ethics application 07/H1003/161+5 (updated in 18/NW/0092) and approval for the work under Manchester Cancer Research Centre Biobank Access Committee application 13_RIMA_01. Barcelona cohort samples were subjected to the ethical committee of Hospital Clínic of Barcelona approval (registry HCB/2015/1032). Data and samples from Leeds were collected in a study named 'Developing a blood test of immunity in illness: a study examining the peripheral blood transcriptome in patients with cancer, autoimmune disease, immunodeficiency or iatrogenic immune suppression' (research ethics committee reference 15/NW/0933). Informed written consent was obtained for collection of samples and data, sharing anonymized data and working with collaborators whether academic or commercial.

Inclusion criteria. Patients who fulfilled the following criteria were eligible for the analysis: (1) histologically or cytologically confirmed non-resectable advanced (stage 3 or 4) cutaneous melanoma, (2) treatment with ICB (nivolumab or pembrolizumab) or a combination of ipilimumab and nivolumab at the recommended dose as a first-line immune checkpoint inhibitor, (3) 18 years of age or older and (4) availability of baseline characteristics presented in Table 1.

Assessment of treatment outcomes. Response to ICB was classified according to RECIST v1.1 criteria. Based on radiographic response, patients were classified as responders (complete response, partial response and stable disease), or nonresponders (progressive disease).

Clinical endpoints were defined as PFS12 and OS. PFS was defined as the time from the initial immunotherapy to disease progression. OS was defined as time in months from initiation of treatment to occurrence of death from any cause. IrAEs, including colitis, were assessed using the CTCAE version 5 (19). Side effects that were clearly of non-immune etiology were excluded.

Sample and data collection. Patients received oral and written instructions regarding the stool collection procedure. Patients within PRIMM-UK and PRIMM-NL were requested to collect approximately 3–5 ml plain feces using a collection kit that could be used at home and then store the sample in their freezer directly after collection. PRIMM-NL samples were transported to the hospital in a frozen insulated cooling bag to prevent thawing. Due to the geographic dispersal of PRIMM-UK patients, samples were collected and placed in Thermo Fisher Scientific kits and sent by special post to the laboratory at King's College London. After arrival in the hospital, the samples were directly stored at -80°C . Plain stool samples from the Manchester cohort were either collected on site at the hospital and stored directly at -80°C within 4–6 h of collection or collected in sample containers and sent by special post to the laboratories of CRUK Manchester Institute and stored directly at -80°C upon arrival. Patients within the Barcelona cohort used the OMNIgene GUT collection kit (DNA Genotek). Fecal DNA was extracted from 1 to 14 days after sample collection using the PowerFecal DNA Isolation Kit (previously MoBio, currently Qiagen) and kept frozen until needed. Patients from Leeds also collected stool at home using the OMNIgene GUT collection kit (DNA Genotek), and samples were returned to the research nurse.

Baseline demographics, including sex, age, body mass index (BMI), Eastern Cooperative Oncology Group (ECOG) performance status and medication use, were collected, along with tumor staging and previous anti-cancer therapy data. Demographic data were collected as part of a screening visit up to 14 days before ICB treatment began. All baseline antibiotics or PPI use within 3 months of commencing ICI treatment was documented. Tumor staging took place up to 1 month before the start of treatment.

Radiological evaluation, consisting of a computed tomography (CT) scan of the thorax, abdomen and pelvis and magnetic resonance imaging of the brain, was performed at baseline (that is, before the first dose of immunotherapy). A small number of patients had positron emission tomography scans with a CT component. Follow-up radiological evaluation was performed every 10–14 weeks as long as the patient received systemic therapy. Additional CT and/or magnetic resonance imaging scans were performed when there was suspicion of progression. If the first radiological evaluation after the start of therapy was inconclusive, then a confirmatory scan was performed 4–12 weeks later.

Metagenomics processing

DNA extraction and sequencing. DNA was isolated for all cohorts at King's College London using Thermo Fisher Scientific's MagMax Core protocols for nucleic acid purification and mechanical lysis. Samples with a high-quality DNA profile ($>15\text{ ng }\mu\text{l}^{-1}$ of DNA) were further processed. Sequencing libraries were prepared using the Illumina Nextera DNA Flex Library Prep Kit according to the manufacturer's protocols. Libraries were multiplexed using dual indexing and sequenced for 300 bp paired-end reads using the Illumina NovaSeq6000 platform according to the manufacturer's protocols. We obtained a total of 1,283 Gb with an average of 53,919,210 reads per sample before quality control and pre-processing.

Metagenome quality control and pre-processing. Shotgun metagenomic sequencing was performed at the NGS Core Facility at University of Trento. The quality of all sequenced metagenomes was controlled using the pre-processing pipeline implemented in ref. 57. Of all the samples collected across the five observational cohorts, we considered those that passed all the quality control steps of the metagenomic sequencing pipeline and had more than 1 Gb of sequencing data. This resulted in a total of 447 samples from 195 patients that were then subjected to strict quality control and were processed into taxonomic and predicted pathway abundances.

Microbiome taxonomic and functional potential profiling. Taxonomic and functional metagenomic profiling was performed using MetaPhlan4¹⁷ with the vJan21 SGB database release and HuMAN3³⁸ with default parameters. Before prevalence filtering (see below), we identified a total of 2,223 microbial SGBs and 518 microbial pathways.

Selection of independent variables for the longitudinal model. We were interested in modeling study visit varying intercept and slopes for patients with PFS ≥ 12 and PFS < 12 months, respectively, in three main clinical contexts: (1) the type of immunotherapy patients received (that is, mono versus combination therapy), (2) if patients had developed any grade of ICB-induced colitis (no versus yes) and (3) if patients received concomitant PPIs (no versus yes). Beyond these three independent variables, we also controlled for previous antibiotics use, previous BRAF or MEK-targeted therapy, time since first injection (in days), cancer center, other forms of irAEs (that is, not colitis), age, sex and BMI. We also included a patient identifier to account for the repeated measurements. In the end, the included variables represented a balance between (1) minimizing collinearity between independent variables, (2) loss of patient samples due to missingness in independent variables and (3) the number of included independent variables versus the number of modeled samples. These selection criteria resulted in 408 samples from 175 patients.

Prevalence filtering of microbiome taxonomic and functional profiles. We retained microbial features that were present in at least 20% of the baseline samples, which also had a prevalence of at least 10% among the longitudinal samples. Applying this stringent filtering criterion, we retained in the 408 samples; 434 and 395 microbial SGBs and pathways, respectively. This was done using phyloseq (v.1.42.0) and tidyverse (v.2.0.0) R packages.

Independent melanoma cohorts for validation. To validate the balance described in Fig. 2a, we downloaded the raw sequences from six publicly available melanoma cohorts (three using radiographic response based on RECIST1.1 criteria, one using PFS12 and two using both RECIST and PFS12) that characterized gut microbiome composition at baseline (Supplementary Table 6). We kept the response definition used in the original publication. One of the cohorts⁵ also characterized gut microbiome composition within 4 months after the start of ICB. We treated these pre- and post-ICB samples from ref. 5 as two cohorts. We re-processed the raw sequences using MetaPhlan4 (using the same database and settings as described above) and computed the balance (Fig. 2a) for all samples in each independent cohort. Not all SGBs were present in all independent cohorts. For example, we did not find taxon GGB1420 SGB1957 (SGB1957) in any of the independent cohorts after 10% prevalence filtering (see Supplementary Table 16 to see which SGBs were missing in each independent cohort). To test whether the balance could predict response anew in each independent cohort, we fit a simple logistic model [glm(response_definition ~ balance_score, family = 'binomial')] to all samples in each cohort and computed the AUC (on the training data, as we fit all samples). We could not include any other independent variables in the models because most cohorts did not report information such as age, sex, BMI or other clinical variables.

Statistical analysis

Compositional data analysis. Metagenomic sequencing produces compositional data, which means that information can only be obtained in the form of relative abundances that are independent of the total microbial load in a given sample. As a result, an increase in one microbial feature (for example, a taxon or metabolic pathway) relative abundance necessarily requires an equivalent decrease in the relative abundance of the remaining community of features present in the same sample. If this statistical property is not accounted for, the likelihood

of introducing false positives in differential abundance analysis^{59,60} and negative correlation biases in correlation-based analysis^{61,62} increases heavily. While standard statistical methodology assumes that the analyzed data are represented by variables free to vary from $-\infty$ to ∞ within Euclidean geometry, compositional data occupy the simplex that is a restricted space where variables are strictly positive and vary from 0 to 1 or 0 to 100, if data are represented as proportions or percentages (such as relative abundances), respectively. A log ratio transformation maps the simplex to Euclidean real space (that is, the Aitchison geometry) where standard statistical methodology can be applied. There are several available log ratio transformations, each using a different reference frame (that is, the denominator). For example, the additive and centered log ratio (alr and clr, respectively) transformation is defined as

$$X_{\text{alr}} = \left[\log\left(\frac{x_1}{x_D}\right), \log\left(\frac{x_2}{x_D}\right), \dots, \log\left(\frac{x_{D-1}}{x_D}\right) \right] \quad (1)$$

$$X_{\text{clr}} = \left[\log\left(\frac{x_1}{g(x)}\right), \log\left(\frac{x_2}{g(x)}\right), \dots, \log\left(\frac{x_D}{g(x)}\right) \right] \quad (2)$$

where $x = [x_1, x_2, x_3, \dots, x_D]$ denotes a sample (that is a composition) containing D 'counted' microbial features. In the alr transformation (equation (1)), the choice of the denominator or the reference frame is arbitrary and could represent any specified feature. In the clr transformation (equation (2)), however, the denominator is defined by the geometric mean $g(x)$ of the focal sample, or put simply, the 'average' feature in the focal sample.

Differential ranking

There already exist several developed methods to find changes in compositional data between cases and controls that avoid the biases caused by the compositional nature of metagenomic sequencing data (for example, ALDEx2⁶³, ANCOM⁶⁴ and Gneiss⁶⁵). What these methods typically have in common is that they internally use some log ratio transformation, which is conserved regardless of whether the data are relative or absolute. A recent approach called differential ranking is robust to the choice of the alr reference feature, and ranks produced from relative abundances are identical to the ranks of absolute abundances^{66,67}. More specifically, the term 'differential' refers to the logarithm of the fold change in abundance of a microbial feature between cases and controls. Differential rankings can therefore be used to detect differentially abundant features knowing that the results are not affected by the compositional nature of the data. It is important to note, however, that high-ranking (positive) features have not necessarily increased in absolute terms between the cases compared to the controls but can still have decreased, although to a lesser extent than the lower-ranking features.

A logistic normal model to estimate differential rankings from proportions

Almost all of the methods developed for compositional sequencing data are intended for counts (for example, 16S rRNA gene amplicons). However, if the processed sequencing data are expressed as proportions with unknown sample totals, then these methods may require changes before being applied. The R package fido⁶⁸ (1.0.4) implements a Bayesian multinomial logistic normal regression model called Pibble that can be adapted to model proportions (that is, only fitting the logistic normal model). Furthermore, the coefficients estimated by Pibble can be ranked and interpreted as differential rankings with statistical significance achieved through Bayesian inference^{68,69}. Pibble is constructed to model any observed sequencing counts using a multinomial distribution, with the underlying microbial feature composition as random variables modeled by a logistic normal distribution. More specifically, the observed relative abundances are considered to be drawn from a multinomial distribution parameterized by a set

of proportions (π_j), which have an analogous representation in the alr space, with the transformed variables drawn from a multivariate normal distribution that exists in Euclidean real space^{68,69}. While both the multinomial Dirichlet model and the multinomial logistic normal model can handle over-dispersed count data^{70,71}, the logistic normal model also allows for both positive and negative covariation between microbial features⁶⁹. In short, the Pibble model is defined as follows:

$$Y_j \sim \text{Multinomial}(\pi_j) \tag{3}$$

$$\pi_j = \text{alr}^{-1}(\eta_j) \tag{4}$$

$$\eta_j \sim \mathcal{N}(AX_j, \Sigma) \tag{5}$$

$$A \sim \text{MN}_{(D-1) \times Q}(\Omega, \Sigma, \Gamma) \tag{6}$$

$$\Sigma \sim W^{-1}(\Xi, \nu) \tag{7}$$

with Y representing a $D \times N$ count matrix with the j th column representing a sample (that is composition) containing the D 'counted' (microbial) features (equation (3)). Equation (4) represents a transformation between the multinomial parameters (π_j sum to 1) that exist on the simplex, and the transformed parameters η_j that exist in Euclidean real space. As is common for multinomial regression, Pibble uses the inverse alr transformation (also called the softmax transform in the machine learning literature) to produce a relative abundance matrix (that is, proportions varying between 0 and 1). This also implies that $\eta_j = \text{alr}(\pi_j)$. The Q modeled covariates are included in the $Q \times N$ matrix denoted X . Importantly, equation (5) simply represents a multivariate linear model with X containing the Q modeled covariates, A a matrix containing the corresponding estimated regression coefficients that can be ranked to produce the differential rankings and Σ a $D \times D$ matrix containing the residual covariance between all log ratios. The matrix containing the estimated regression coefficients (that is, A) is modeled as a matrix normal distribution, which is simply a generalization of the multivariate normal distribution capable of describing the covariation between the rows (that is, features Σ) and between the columns (that is, samples, Γ) of A (equation (6)). Finally, Σ is modeled as an inverse Wishart distribution (W^{-1}), which is a common distribution over covariance matrices (equation (7))^{68,69}.

Owing to the large flexibility of the Pibble model, it is possible to directly model sequencing data expressed as proportions (that is, relative abundances) using the logistic normal model (that is, starting from equation (4)). The only drawback of this is that variation in the counts cannot be modeled, but this information is naturally lost once data are normalized (and if the information on sample totals is not kept). Importantly, once the model is fit, the results can be viewed as if any log ratio transform had been used (instead of the alr in equation (4)), including the clr. Lastly, because equation (5) simply represents a multivariate linear model, interactions between predictor variables can also be modeled. Pibble uses the collapse–uncollapse sampler, which was developed particularly for this class of models^{68,69}. We used the same priors as suggested by refs. 68,69.

A linear model with higher-order interactions

We hypothesized that microbial abundances may change over the course of the treatment period because patients received an immunotherapy injection at each treatment visit, thus probably increasing the cumulative effect of the therapy on the gut microbiome across the study period. We further hypothesized that patients with PFS ≥ 12 and PFS < 12 months may exhibit different patterns of change. To model this, we included higher-order interactions, thereby assuming that microbial abundances change linearly across study visits. In equation (5),

we modeled the relationship between X (study visits/cumulative number of treatment injections) and Y (the log ratio value for any given microbial feature) to be contingent not only on Z whether patients achieved PFS ≥ 12 months, but also on the moderator variable W , which in our case represents one of three treatment characteristics of interest. Therefore, the three three-way interactions we modeled all included the same X and Z variables but with a different treatment characteristic of interest (that is, the moderator variable W_{1-3} ; see equation (8)). The different treatment characteristics for W that we modeled were: W_1 , the type of immunotherapy patients received (that is mono versus combination therapy); W_2 , if patients had developed any grade of ICB-induced colitis (no versus yes); and W_3 , if patients received concomitant PPIs (no versus yes). Beyond the different treatment characteristics, we also controlled for whether patients have had previous chemotherapy, time since first injection (in days), the cancer center patients were treated at, whether they experienced other forms of irAEs (that is, not colitis), age, sex and BMI. We also included a patient identifier to account for the repeated measurements. Lastly, before model fitting, all continuous variables (that is, age and BMI) were mean centered, and all 'peripheral' categorical variables (that is, previous therapy, center, other forms of irAEs, patient identification and sex) were coded using weighted sum contrasts (as opposed to treatment contrasts). The latter effectively mean-centers categorical variables with the result being that the intercept represents the average of all independent variables not included in the three-way interactions. To note is that all 175 patients in the main analysis have information on all of these metadata (that is, there is nothing missing/not available).

Without including any of the 'peripheral' independent variables, which we adjusted for (that is, center, time to/since first injection, other forms of irAEs, patient identification, age, sex and BMI), we can write our linear regression model as

$$Y = \beta_0 + \beta_1 X + \beta_2 Z + \beta_3 XZ + \underbrace{\beta_4 W_1 + \beta_5 XW_1 + \beta_6 ZW_1 + \beta_7 XZW_1}_{\text{Combination therapy}} + \underbrace{\beta_8 W_2 + \beta_9 XW_2 + \beta_{10} ZW_2 + \beta_{11} XZW_2}_{\text{Colitis}} + \underbrace{\beta_{12} W_3 + \beta_{13} XW_3 + \beta_{14} ZW_3 + \beta_{15} XZW_3}_{\text{PPI}} \tag{8}$$

where Z and W_{1-3} are binary variables dummy coded to be either 0 or 1, always with 0 as the reference category. Thus, the β_2 coefficient for Z (PFS12: 0 is PFS < 12 , 1 is PFS ≥ 12) represents the value when all treatment characteristics of interest (W_{1-3}) are at their reference level (that is, monotherapy (W_1), no colitis (W_2) and no PPIs (W_3)) and when the independent variable X has a value of zero (that is, baseline). We can further rewrite equation (8) to illustrate that the relationship between X and Y is conditional on Z and W_{1-3} as follows:

$$Y = \underbrace{(\beta_0 + \beta_2 Z + \beta_4 W_1 + \beta_6 ZW_1 + \beta_8 W_2 + \beta_{10} ZW_2 + \beta_{12} W_3 + \beta_{14} ZW_3)}_{\text{intercepts}} + \underbrace{(\beta_1 + \beta_3 Z + \beta_5 W_1 + \beta_7 ZW_1 + \beta_9 W_2 + \beta_{11} ZW_2 + \beta_{13} W_3 + \beta_{15} ZW_3)}_{\text{slopes}} X \tag{9}$$

where the first and second parentheses represent the intercepts and the slopes graphing Y against X .

Post hoc contrasts to compute the comparisons of interest

To create the relevant comparisons between cases and controls, we constructed so-called post hoc contrasts (linear combinations of coefficients) directly from the fitted model. To compute these, we first constructed reference grids (Supplementary Information), which contain all relevant combinations of the categorical independent variables that we wanted to average over. Based on these reference grids, we computed marginal means of cases and controls, which we then could statistically compare. Because we already mean centered

all ‘peripheral’ independent (continuous and categorical) variables, we only consider the coefficients associated with the treatment characteristic of interest (W_{1-3}), which is shown in equation (8). The post hoc contrasts we computed were (1) PFS ≥ 12 versus PFS < 12 months, (2) colitis versus no colitis, (3) PFS ≥ 12 months with and without colitis, (4) patients on combination versus monotherapy with colitis, (5) PFS ≥ 12 versus PFS < 12 months on monotherapy without colitis and no PPIs, (6) PFS ≥ 12 versus PFS < 12 months on combination therapy without colitis and no PPIs and (7) PFS ≥ 12 versus PFS < 12 months on PPIs, monotherapy and without colitis. In Supplementary Information, we show the mathematical procedure to compute these post hoc contrasts for (1), (2) and (3), but the same logic applies when computing to the remaining contrasts.

Balance analysis

A balance is a type of log ratio defined as the ratio between the geometric means of two subsets of features^{72,73}. Following the definition in ref. 73, mathematically a balance is defined as follows. Let $X = (X_1, X_2, X_3, \dots, X_k)$ be a sample with k features. Given two non-overlapping subsets of features in X denoted by X_+ and X_- , indexed by I_+ and I_- , and comprising k_+ and k_- , the balance between X_+ and X_- is defined as the log ratio of the geometric mean of the two subsets of features as follows:

$$B(X_+, X_-) = \log \left(\frac{\left(\prod_{i \in I_+} X_i \right)^{1/k_+}}{\left(\prod_{j \in I_-} X_j \right)^{1/k_-}} \right). \quad (10)$$

Expanding the logarithm, we can simplify the above equation as

$$B(X_+, X_-) = \frac{1}{k_+} \sum_{i \in I_+} \log X_i - \frac{1}{k_-} \sum_{j \in I_-} \log X_j. \quad (11)$$

Note that we have removed the normalization constant $\frac{1}{k}$ from the original definition as it is later shown by ref. 74 to be unnecessary. Using the relative abundances of the focal SGBs, we computed different balances using the above mathematical formula implemented in custom-written R scripts. Because each balance consists of a selection of SGBs or ‘top hits’ from the longitudinal model that already adjusts for a large number of confounders, the effect of different confounders (for example, cancer center) on each balance score, has already been averaged out.

Survival analysis

To test whether a focal balance was associated with OS at baseline, we used the multivariable Cox proportional hazard regression model as implemented in the `coxph()` function in the R package `survival` (3.5-5). We either considered the start of therapy to (1) death from any cause (OS) or (2) progression or death from any cause (PFS) as the time-to-event data. If patients were event-free (that is, alive and/or progression-free) at the last follow-up (28 March 2023), they were right censored. We used these models to estimate HRs including their 95% confidence intervals (CIs) for OS, adjusting for sex, age, BMI, PPI, antibiotics use, previous chemotherapy, colitis and other irAEs. We had $n = 146$ patients for which these data were complete (that is, no missings). The proportional hazard assumption was checked testing the trend of the Schoenfeld residuals with the `cox.zph()` function in the `survival` package (3.5-5). We did not observe any violations in this assumption. Finally, survival curves were estimated using the Kaplan–Meier method as implemented in the `survfit2()` function in the R package `ggsurvfit` (0.3.0).

Reporting summary

Further information on research design is available in the Nature Portfolio Reporting Summary linked to this article.

Data availability

The longitudinally profiled metagenomes have been deposited in the European Nucleotide Archive under accession number [PRJEB70966](https://doi.org/10.1038/s41591-024-02803-3). Baseline samples are already deposited under accession number [PRJEB43119](https://doi.org/10.1038/s41591-024-02803-3). All MetaPhlan4 and HUMAnN3 profiles will also be available within the latest version of curated MetagenomicData (<https://bioconductor.org/packages/curatedMetagenomicData>). All relevant patient data used in this study can be requested by emailing the first author (bjork.johannes@gmail.com). The six previously published studies used for validation are available under accession numbers: [PRJNA770295](https://doi.org/10.1038/s41591-024-02803-3), [PRJNA541981](https://doi.org/10.1038/s41591-024-02803-3), [PRJNA762360](https://doi.org/10.1038/s41591-024-02803-3), [PRJNA399742](https://doi.org/10.1038/s41591-024-02803-3), [PRJNA397906](https://doi.org/10.1038/s41591-024-02803-3), [PRJEB22893](https://doi.org/10.1038/s41591-024-02803-3) and [PRJEB22894](https://doi.org/10.1038/s41591-024-02803-3) (see Supplementary Table 6).

Code availability

All code is available in the first author’s GitHub page (<https://github.com/johannesbjork/Longitudinal-gut-microbiome-changes-in-ICB-treated-advanced-melanoma>) and mirrored at WeersmaLab (<https://github.com/WeersmaLabIBD>).

References

- OncolifeS Oncological Life Study: living well as a cancer survivor (University Medical Center Groningen, 2022)
- SegataLab. *GitHub* <https://github.com/SegataLab/preprocessing> (2023).
- Beghini, F. et al. Integrating taxonomic, functional, and strain-level profiling of diverse microbial communities with bioBakery 3. *eLife* **10**, e65088 (2021).
- Hawinkel, S., Mattiello, F., Bijmens, L. & Thas, O. A broken promise: microbiome differential abundance methods do not control the false discovery rate. *Brief. Bioinform.* **20**, 210–221 (2019).
- Gloor, G. B., Macklaim, J. M., Pawlowsky-Glahn, V. & Egozcue, J. J. Microbiome datasets are compositional: and this is not optional. *Front. Microbiol.* **8**, 2224 (2017).
- Jian, C., Luukkonen, P., Yki-Järvinen, H., Salonen, A. & Korpela, K. Quantitative PCR provides a simple and accessible method for quantitative microbiota profiling. *PLoS ONE* **15**, e0227285 (2020).
- Gloor, G. B., Wu, J. R., Pawlowsky-Glahn, V. & Egozcue, J. J. It’s all relative: analyzing microbiome data as compositions. *Ann. Epidemiol.* **26**, 322–329 (2016).
- Fernandes, A. D. et al. Unifying the analysis of high-throughput sequencing datasets: characterizing RNA-seq, 16S rRNA gene sequencing and selective growth experiments by compositional data analysis. *Microbiome* **2**, 15 (2014).
- Mandal, S. et al. Analysis of composition of microbiomes: a novel method for studying microbial composition. *Microb. Ecol. Health Dis.* **26**, 27663 (2015).
- Morton, J. T. et al. Balance trees reveal microbial niche differentiation. *mSystems* **2**, e00162–16 (2017).
- Lin, H. & Peddada, S. D. Analysis of microbial compositions: a review of normalization and differential abundance analysis. *NPJ Biofilms Microbiomes* **6**, 60 (2020).
- Morton, J. T. et al. Establishing microbial composition measurement standards with reference frames. *Nat. Commun.* **10**, 2719 (2019).
- Silverman, J. D., Roche, K., Holmes, Z. C., David, L. A., & Mukherjee, S. R package `fido` (v.1.0.4). *GitHub* <https://jsilve24.github.io/fido/> (2022).
- Silverman, J. D., Roche, K., Holmes, Z. C., David, L. A. & Mukherjee, S. Bayesian multinomial logistic normal models through marginally latent matrix-T processes. *J. Mach. Learn. Res.* **23**, 1–42 (2022).
- Chen, J. & Li, H. Variable selection for sparse dirichlet-multinomial regression with an application to microbiome data analysis. *Ann. Appl. Stat.* <https://doi.org/10.1214/12-AOAS592> (2013).

71. Xia, F., Chen, J., Fung, W. K. & Li, H. A logistic normal multinomial regression model for microbiome compositional data analysis. *Biometrics* **69**, 1053–1063 (2013).
72. Calle, M. L., Pujolassos, M. & Susin, A. coda4microbiome: compositional data analysis for microbiome cross-sectional and longitudinal studies. *BMC Bioinform.* **24**, 82 (2023).
73. Rivera-Pinto, J. et al. Balances: a new perspective for microbiome analysis. *mSystems* **3**, e00053–18 (2018).
74. Gordon-Rodriguez, E., Quinn, T. P. & Cunningham, J. P. Learning sparse log-ratios for high-throughput sequencing data. *Bioinformatics* **38**, 157–163 (2021).

Acknowledgements

This work was supported by the Seerave Foundation. The work was also supported by the European Research Council (ERC-STG project MetaPG to N.S.), MIUR ‘Futuro in Ricerca’ (grant RBF13EWWI_001 to N.S.), the European Horizon 2020 program (ONCOBIOME-825410 project and MASTER-818368 project to N.S.), the National Cancer Institute of the National Institutes of Health (grant 1U01CA230551 to N.S. and L.W.), the Premio Internazionale Lombardia e Ricerca 2019 (to N.S.), the Spanish Fondo de Investigaciones Sanitarias (grants PI15/00716 and PI15/00956) of the Instituto de Salud Carlos III, Spain, co-financed by European Development Regional Fund ‘A way to achieve Europe’ to E.R.D.F., the Wellcome Trust (grant 100282/Z/12/Z to N.C.-L.), and the Dutch Cancer Society (grant 10034 POINTING to E.G.E.d.V.). N.C.-L. is the recipient of a PhD fellowship (FPU17/05453) from the Ministerio de Educación, Cultura y Deportes, Spain. The Leeds group was supported by the Medical Research Council (grant MR/MO19012/1). S.V. was supported by a Harry J. Lloyd Charitable Trust Career Development Award. We acknowledge the Seerave Foundation, which funded this work and many other projects investigating the gut microbiome in human health and disease. We thank the team of the NGS Core Facility at University of Trento for support in sample preparation and for metagenomic sequencing and the high-performance computing team at the University of Trento. We also thank Oncobiome and the Institut Gustave Roussy for their involvement and support of our initiative. The collection of samples from the Hospital Clínic in Barcelona was funded by grant PI15/00716 from Fondo de Investigaciones Sanitarias, Instituto de Salud Carlos III, Spain. Funders did not influence the study design or data analysis. We also thank H. Donker and D. Neijzen for providing feedback on the statistical models. Lastly, we would like to thank all the patients who selflessly took the time to collect samples for this project.

Author contributions

K.A.L., L.A.B., N.C.-L., P.S.-B. and M. Harland collected the clinical data. N.D., K.B., M.P. and S.V. provided organizational and scientific

assistance relating to sample collection and processing of the samples. A.M.T., P.M., F. Armanini, F. Asnicar, A.B.-M., F.P., M.Z. and A.V. supervised by N.S., were responsible for the bioinformatics pipeline. J.R.B. performed all statistical analyses, and J.R.B. and L.A.B. wrote the paper supervised by G.A.P.H. and R.K.W. E.G.E.d.V., R.S.N.F., G.A.P.H. and R.K.W. reviewed all versions of the paper. All authors reviewed the manuscript before submission. R.B., P.L., R.M., J.N.-B., H.M.S., M. Harries, E.G.E.d.V., P.N., R.S.N.F., S.P., V.B., T.D.S., G.A.P.H. and R.K.W. provided supervision over the studies and collection protocols within which samples were collected. All authors approved the final manuscript.

Competing interests

R.K.W. acted as a consultant for Takeda; received unrestricted research grants from Takeda, Johnson & Johnson, Tramedico and Ferring; and received speaker fees from MSD, AbbVie and Janssen Pharmaceuticals. E.G.E.d.V. reports an advisory role at Daiichi Sankyo, NSABP and Sanofi (paid to University Medical Center Groningen) and research funding from Amgen, AstraZeneca, Bayer, Chugai Pharma, CytomX Therapeutics, G1 Therapeutics, Genentech, Nordic Nanovector, Radius Health, Regeneron, Roche, Servier and Synthron (paid to University Medical Center Groningen). S.P. received speaker fees from Ammirall, BMS, ISDIN, La Roche Posay, Leo Pharma, Regeneron, Roche and Sanofi; acted as advisory board member of Ammirall, ISDIN, La Roche Posay, Pfizer, Roche, Regeneron, Sanofi and Sun Pharma; and received research funding from Abbie, AMGEN, ISDIN, La Roche Posay, Leo Pharma and Novartis. R.B. has received honoraria from, and sits on advisory boards of, Novartis, BMS and MSD. The other authors declare no competing interests.

Additional information

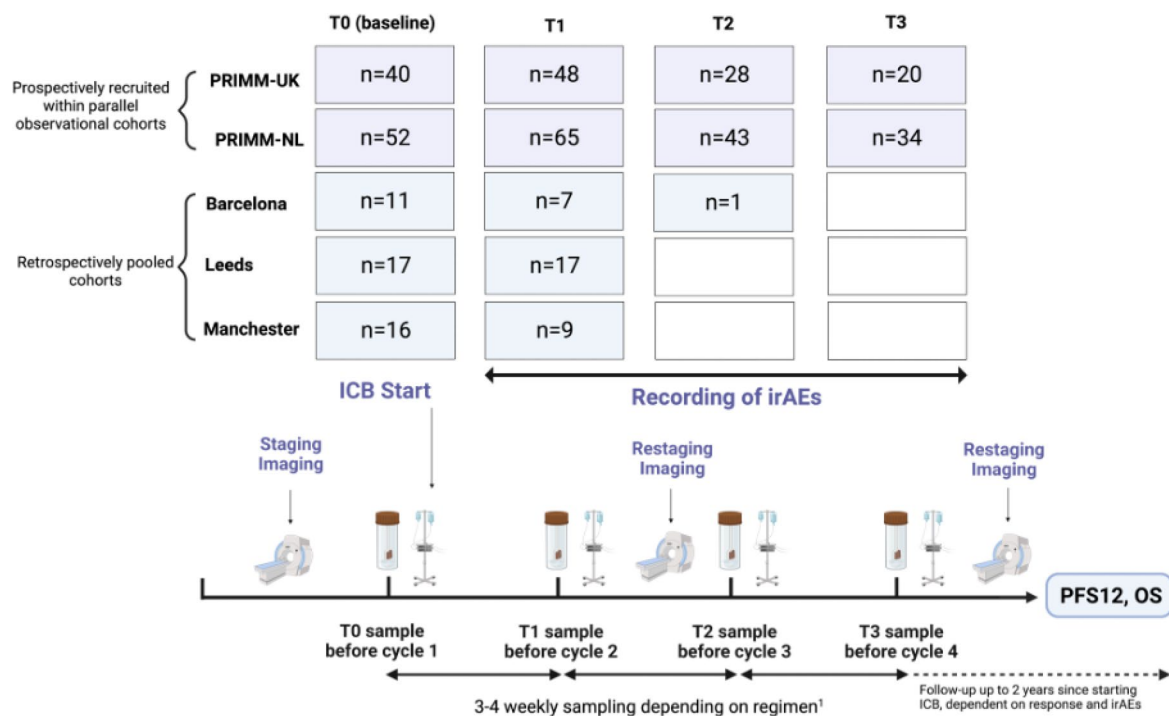
Extended data is available for this paper at <https://doi.org/10.1038/s41591-024-02803-3>.

Supplementary information The online version contains supplementary material available at <https://doi.org/10.1038/s41591-024-02803-3>.

Correspondence and requests for materials should be addressed to Johannes R. Björk or Rinse K. Weersma.

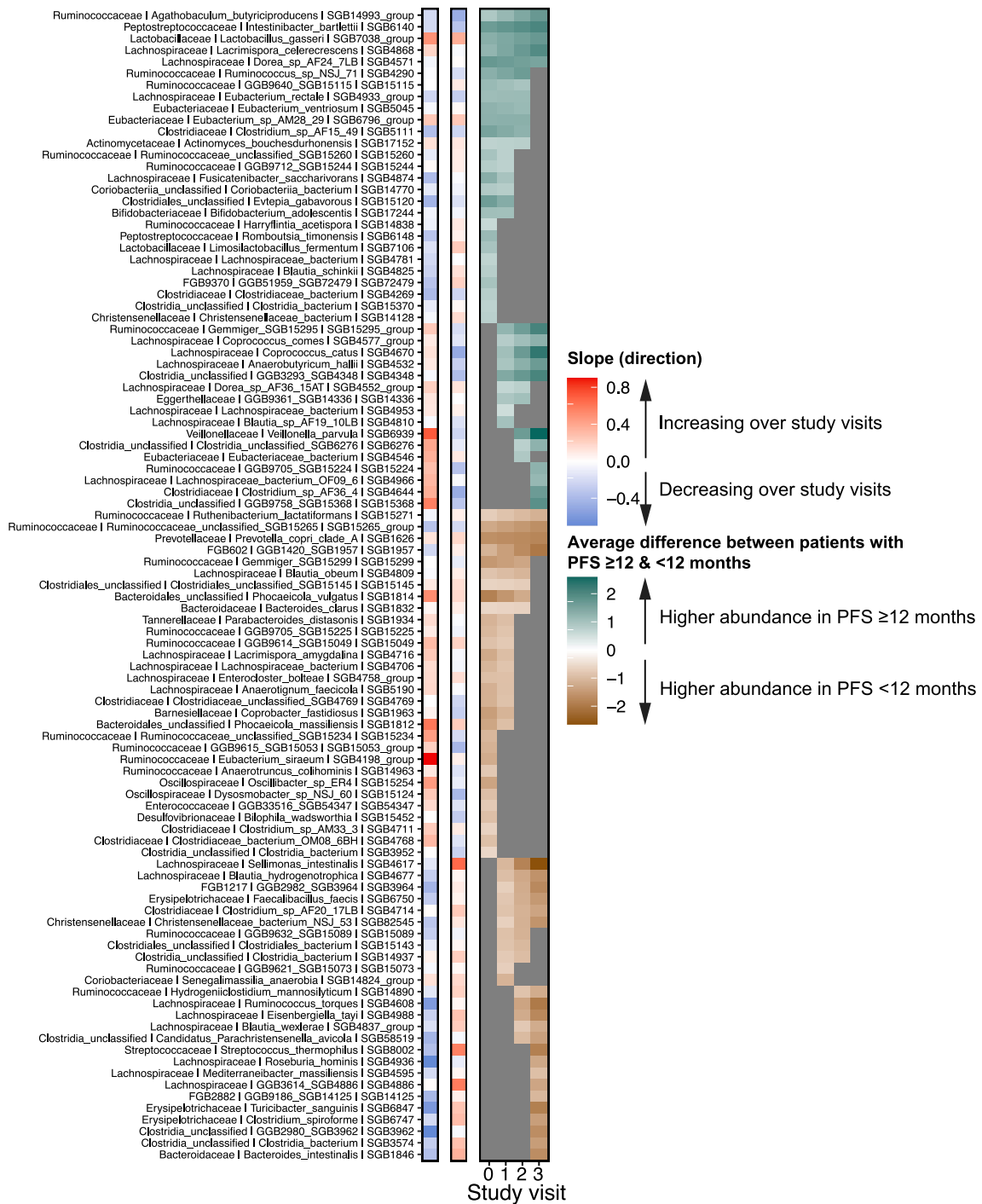
Peer review information *Nature Medicine* thanks Diwakar Davar, Jonathan Peled, and Saman Maleki Vareki for their contribution to the peer review of this work. Primary Handling Editor: Alison Farrell, in collaboration with the *Nature Medicine* team.

Reprints and permissions information is available at www.nature.com/reprints.

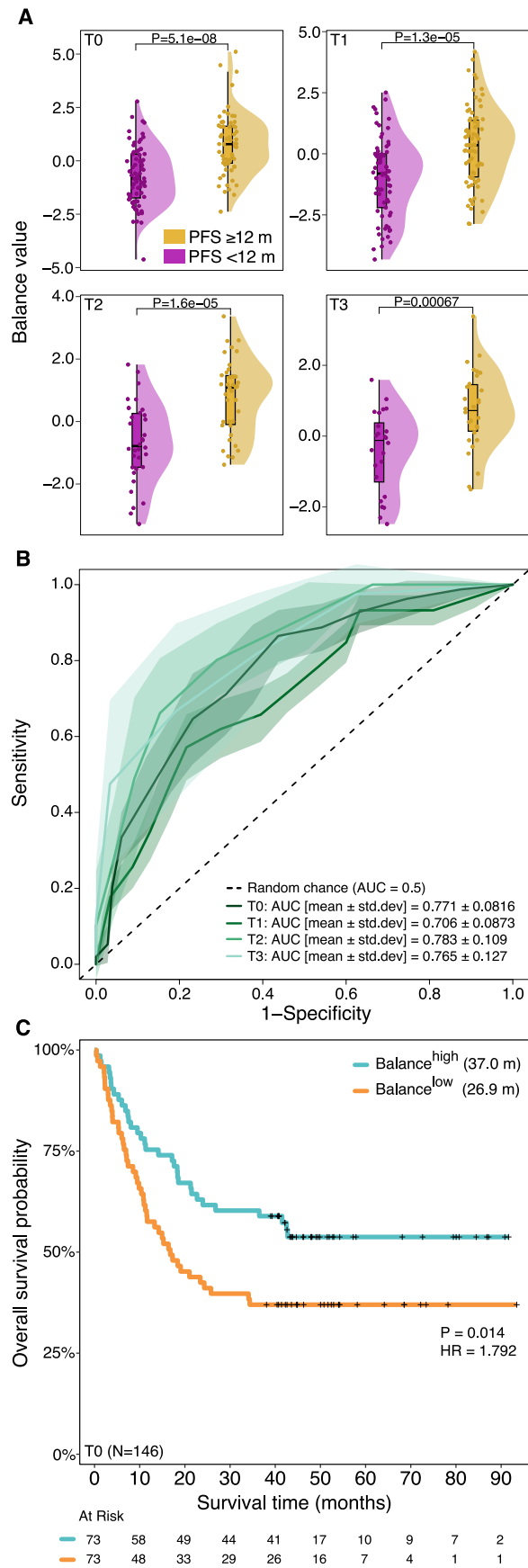


Extended Data Fig. 1 | Study description with sample numbers across study visits. Samples were collected within 5 sub-cohorts: two prospectively recruited within parallel observational studies (The PRIMM cohorts), and three retrospectively pooled cohorts. Fecal samples were collected at 4 timepoints: at baseline (T0) and at every treatment cycle (T1 to T3) over a period of 12 weeks. The time between two samples was 3 or 4 weeks, depending on the treatment regimen, with Ipilimumab/Nivolumab combination therapy and Pembrolizumab monotherapy administered 3-weekly and Nivolumab monotherapy administered 4-weekly. Treatment continued after the 12 weeks until the patient responded or until the treatment had to pause/stop due to irAEs. Not all subjects provided fecal samples at all study visits. Therefore, gut microbial dynamics were modeled at the level of the population including a random effect for the patient identifier (see Methods). Sample numbers represent patients with complete metadata

(that is, no missingness) for all considered covariates/confounders. For the survival analysis, because we adjusted for a smaller number of covariates/confounders, there were $n = 147$ at baseline (PRIMM-UK = 41; PRIMM-NL = 53; Barcelona = 12; Leeds = 17; Manchester = 24) rather than $n = 136$ as indicated here. Tumor staging by CT or PET-scans was performed at study entry and at regular intervals during treatment. Tumor response was classified using the Response Evaluation Criteria in Solid Tumors (RECIST) v.1. Endpoints were defined as Progression-free survival at 12 months (PFS12) and overall survival (OS). Immune-related adverse events (irAEs) were assessed using the Common Terminology Criteria for Adverse Events (CTCAE) v.5 (see Table 1). ICB, Immune checkpoint blockade; PRIMM, Predicting Response to Immunotherapy for Melanoma With Gut Microbiome and Metabolomics; NL, Netherland; UK, United Kingdom. The figure was generated in [BioRender.com](https://www.biorender.com).



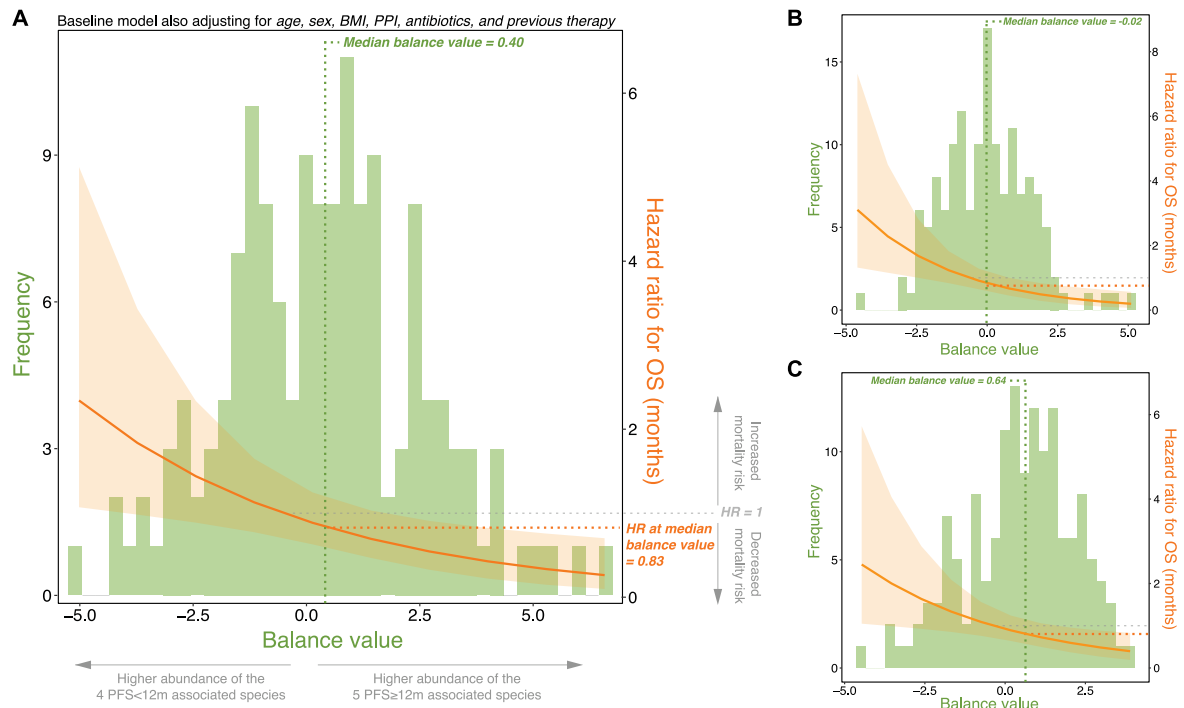
Extended Data Fig. 2 | Extension of Fig. 1. This includes all SGBs, that is, also those that were differentially abundant in only one study visit.



Extended Data Fig. 3 | See next page for caption.

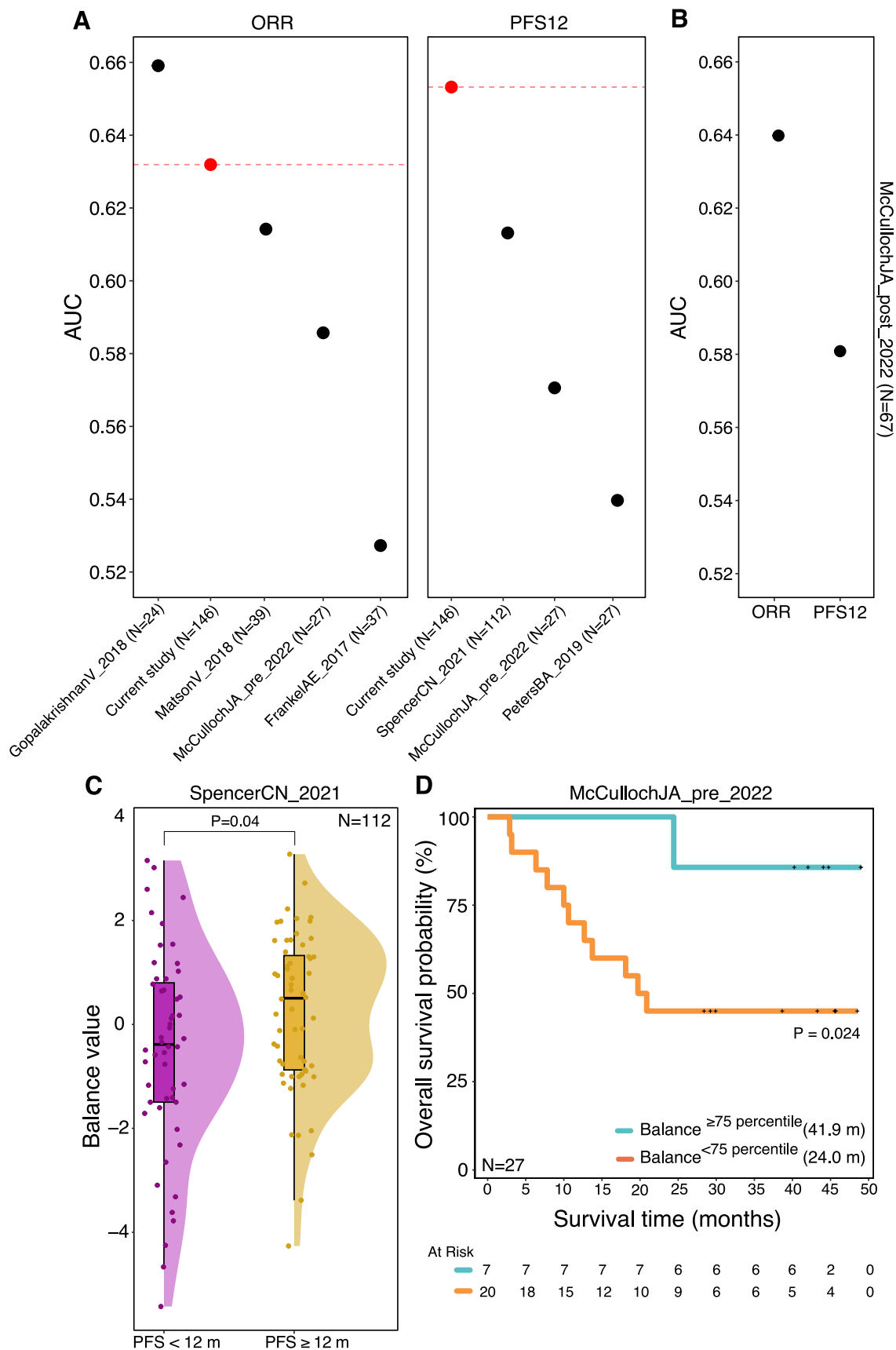
Extended Data Fig. 3 | Extended longitudinal balance. The extended balance has 12 SGBs in the numerator (*A. butyrificiproducens* [SGB14993 group], *I. bartlettii* [SGB6140], *D. sp AF24 7LB* [SGB4571], *L. gasseri* [SGB7038 group], *L. celerecrescens* [SGB4868], *R. sp NSJ71* [SGB4290], *GGB9640* [SGB15115], *E. rectale* [SGB4933 group], *E. entriosum* [SGB5045], *E. sp AM28 29* [SGB6796 group], *Clostridium sp AF15 49* [SGB5111], and *A. bouchedurhonensis* [SGB17152]) and 9 SGBs in the denominator (*R. lactatiformans* [SGB15271], *R. unclassified* [SGB15265 group], *P. copri clade A* [SGB1626], *GGB1420* [SGB1957], *Gemmiger* [SGB15299], *B. obeum* [SGB4809], *Clostridiales unclassified* [SGB15145], *P. vulgatus* [SGB1814], and *B. clarus* [SGB1832]). Panel (A) balance's ability to discriminate between patients with PFS ≥ 12 (n = 83; n₀ = 62; n₁ = 77; n₂ = 38; n₃ =

30) and PFS < 12 (n = 92; n₀ = 74; n₁ = 69; n₂ = 34; n₃ = 24) months across study visits. Boxplots represent minima, Q1, Q2, Q3, and maxima. Panel (B) the balance's predictive ability expressed as the Area Under the Curve (AUC) computed from 100 times repeated five-fold cross-validation (CV). Each line shows, for each study visit, the average across the 100 repeated five-fold CVs with the shaded area representing the 95% confidence interval. Panel (C) Kaplan–Meier curves and multivariable Cox regression analysis of overall survival in 146 patients at baseline (one patient was removed due to missingness in the included predictor variables) according to high (above median) and low (below median) values of the balance after adjusting for age, sex, BMI, previous therapy, PPI and antibiotic use.



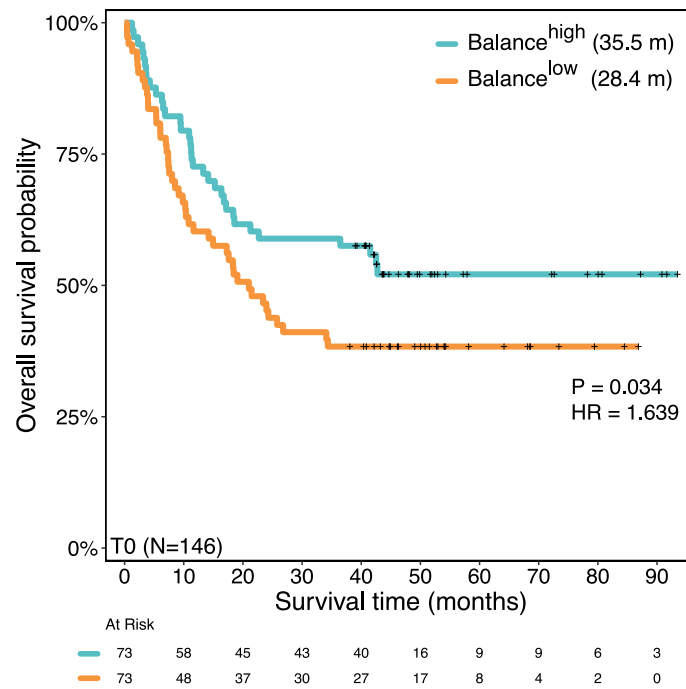
Extended Data Fig. 4 | Treating balances as continuous independent variables. Panel A-C shows a multivariable Cox regression analysis of overall survival (OS) in months for 146 patients at baseline (one patient was removed due to missingness in the included predictor variables) treating (a) the first balance (Fig. 2a), (b) the second balance (that is, the extended longitudinal balance),

and (c) the third balance (that is, the 'baseline only' balance) as a continuous independent variable. While the histograms show the distribution of each balance (right y-axes), each regression line represent the hazard ratio as a smooth function of each balance (left y-axes). All models are adjusted for age, sex, BMI, PPI and antibiotics use, and previous therapy.



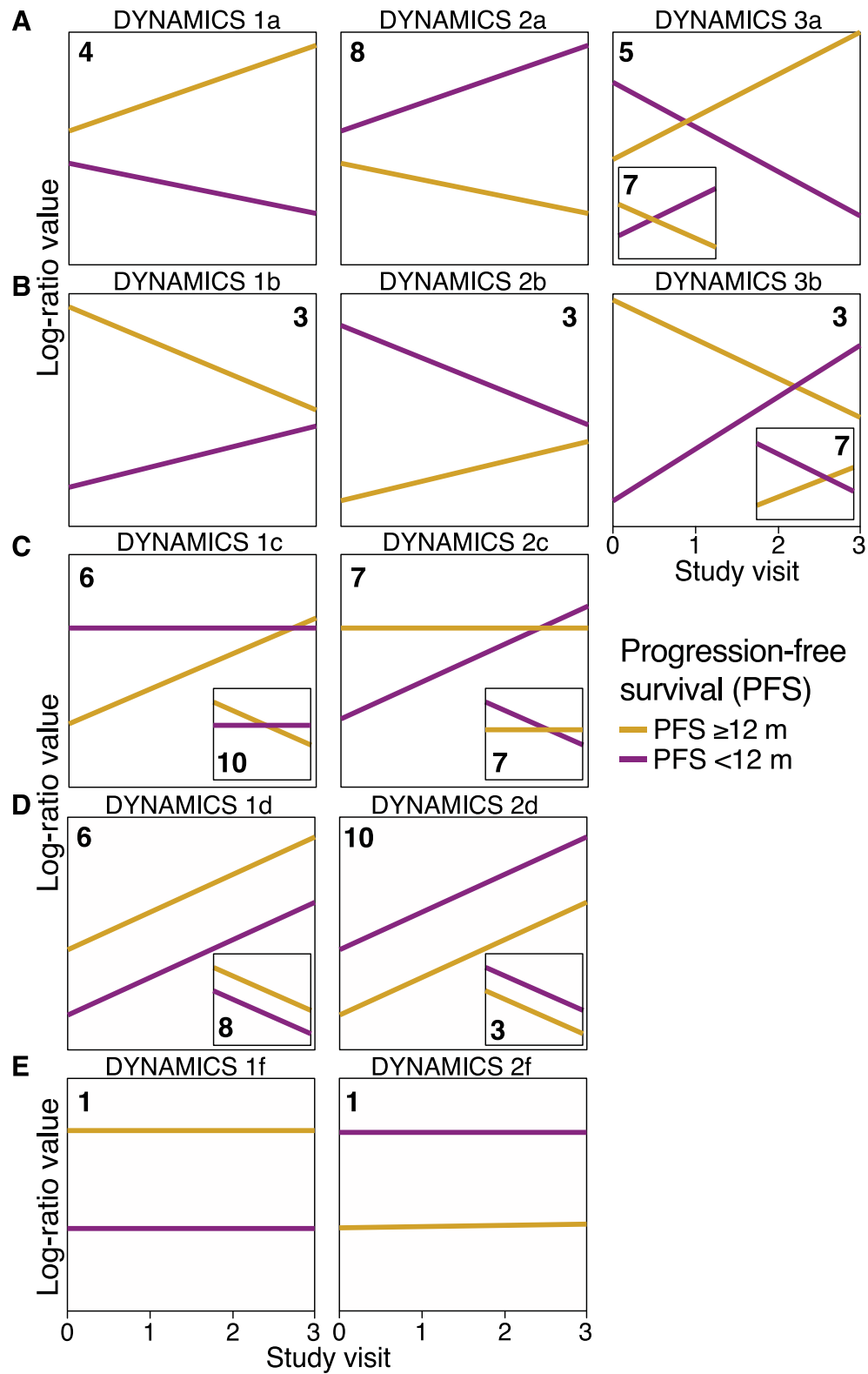
Extended Data Fig. 5 | Generalizability of the longitudinal balance (Fig. 2a) across six independent melanoma cohorts. Panel (A) shows the AUC for each independent baseline cohort, including the current study (in red). Panel (B) shows the AUC for *McCullochJA_2022*'s post-ICB cohort. Panel (C) shows the average difference in the balance score between patients with PFS < 12 months

versus PFS ≥ 12 months from the *SpencerCN_2021* cohort. Finally, panel (D) shows Kaplan-Meier curves and multivariable Cox regression analysis of overall survival (OS) in months from 27 patients from *McCullochJA_2022*'s baseline cohort according to high (≥75 percentile) and low (<75 percentile) values of the balance after adjusting for age, sex, BMI and PPI-use.



Extended Data Fig. 6 | Baseline only balance. A 'baseline only' balance containing the 9 species associated with patients with PFS ≥ 12 months at baseline only in the numerator, and the 11 SGBs associated with patients with PFS < 12 months at baseline only in the denominator (see Fig. 1a). Kaplan-Meier curves

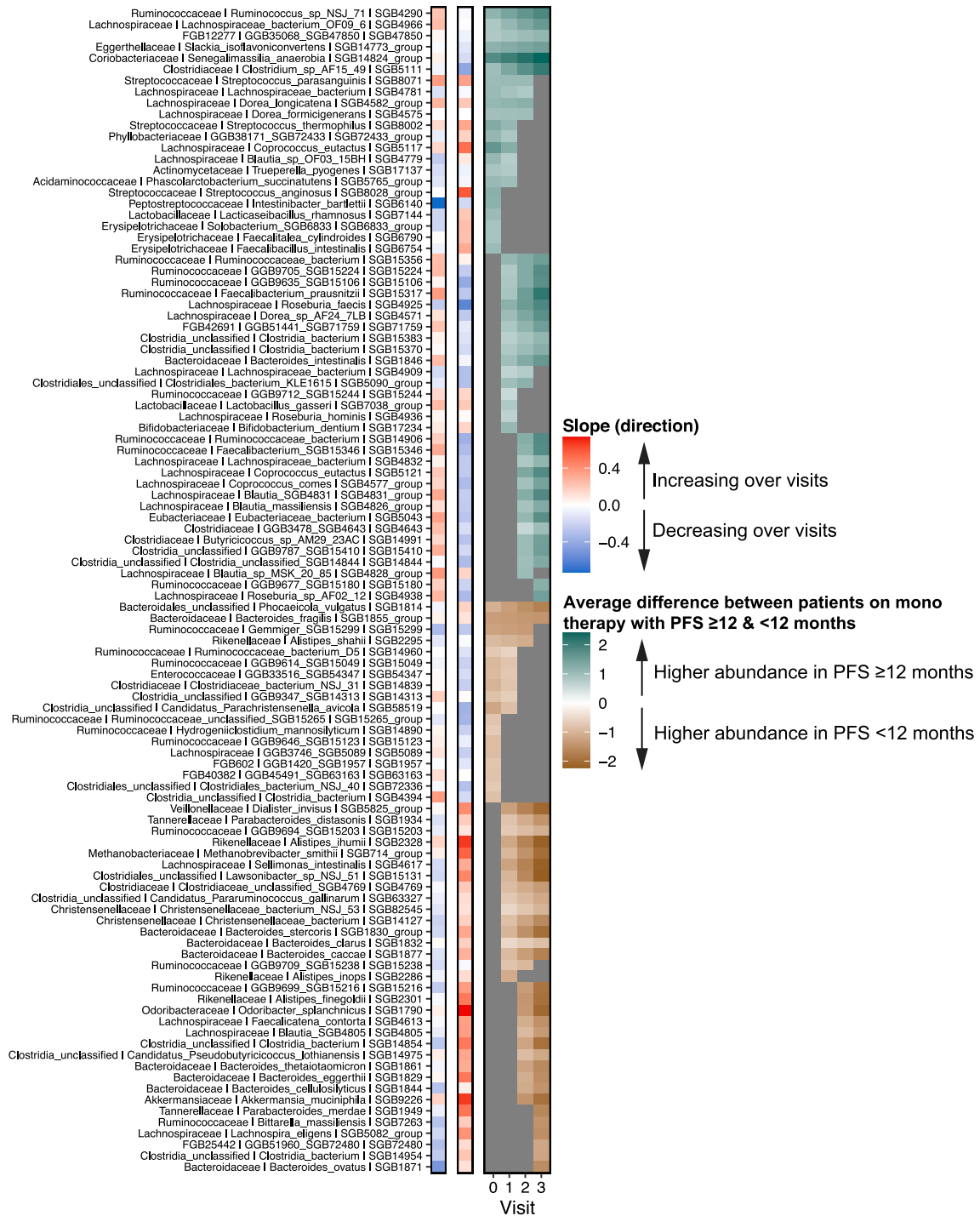
and multivariable Cox regression analysis of overall survival in 146 patients at baseline (one patient was removed due to missingness in the included predictor variables) according to high (above median) and low (below median) values of the balance after adjusting for age, sex, BMI, previous therapy, PPI and antibiotic use.



Extended Data Fig. 7 | See next page for caption.

Extended Data Fig. 7 | Schematic illustration showing the different types of microbial dynamics we observe between patients with PFS ≥ 12 months and PFS < 12 months. Panels A-E are schematic illustrations (that is, cartoons) showing the breakdown of the different types of taxon dynamics we observe in the overall comparison between patients with PFS ≥ 12 months and patients with PFS < 12 months. Yellow and purple slopes correspond to patients with PFS ≥ 12 and PFS < 12 months, respectively. Panel (A) shows dynamics where patients with PFS ≥ 12 and PFS < 12 months are differentially abundant only after T0 (that is, dynamics 1a and 2a). Dynamics 3a is a particular case of dynamics 1a and 2a where the slopes for patients with PFS ≥ 12 and PFS < 12 months intersect. Panel (B) shows dynamics where patients with PFS ≥ 12 and PFS < 12 months are differentially abundant at early but not at late visits (that is, dynamics 1b and 2b).

Dynamics 3b is a special case of dynamics 1b and 2b where the patients with PFS ≥ 12 and PFS < 12 months slopes intersect. Panel (C) shows dynamics where the slope of one of the groups is zero (or close to zero) while the other group is either increasing or decreasing, respectively (that is, dynamics 1c and 2c). In panels (D) and (E), included the inset figures, patients with PFS ≥ 12 and PFS < 12 months exhibit parallel lines (that is, no statistical interactions); Panel 1d and 2d shows dynamics where both patients with PFS ≥ 12 and PFS < 12 months are either increasing or decreasing, respectively, while in panels 1f and 2f, the slopes of patients with PFS ≥ 12 and PFS < 12 months are zero (or close to zero). The number in each plot corresponds to the number of microbial SGBs that follow each type of different dynamics.



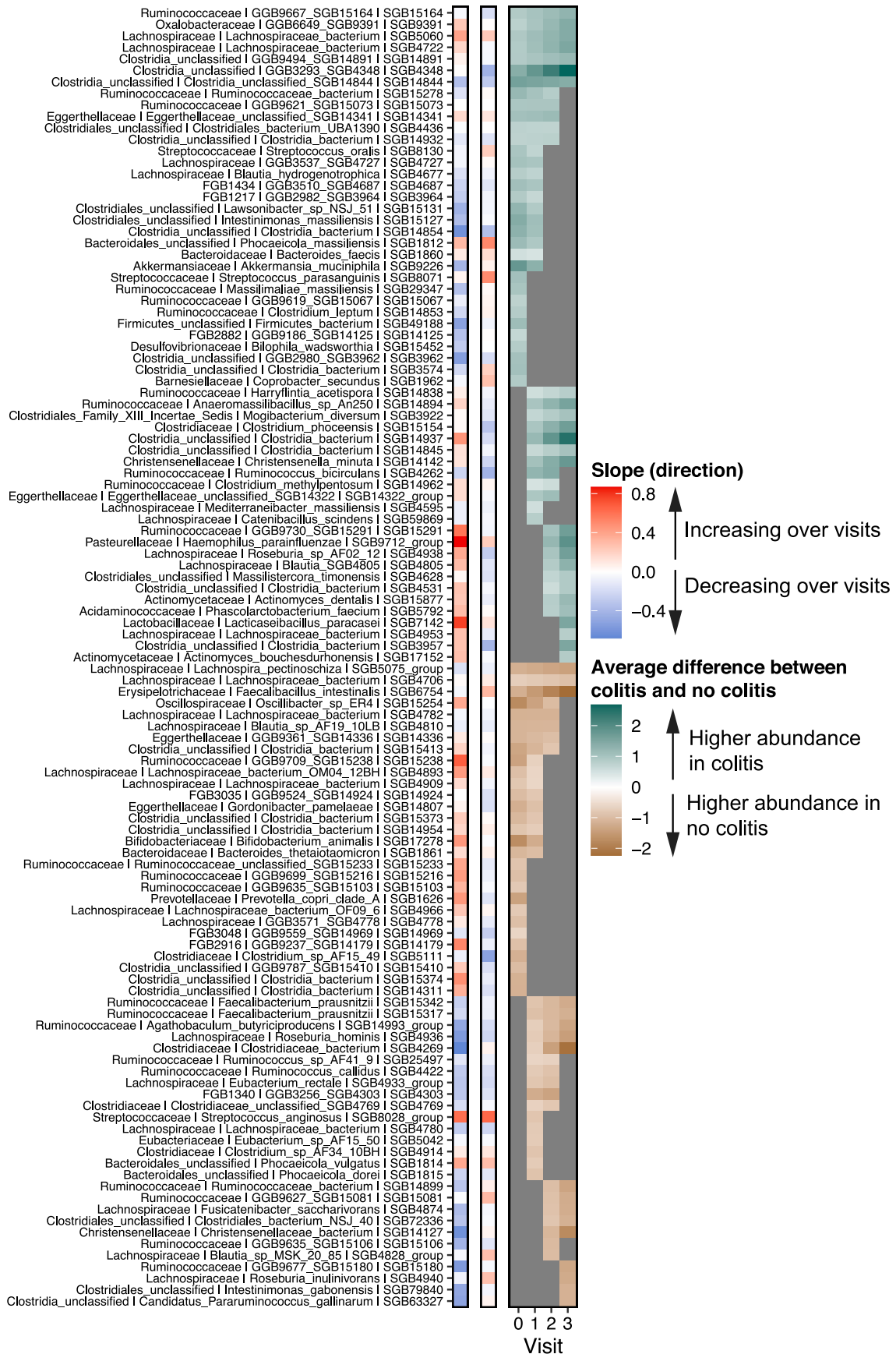
Extended Data Fig. 8 | Patients with PFS ≥ 12 and PFS < 12 months on monotherapy. Panel (A) shows, for each microbial SGB listed, its slopes in patients with PFS ≥ 12 months and PFS < 12 months on monotherapy, respectively. Red and blue colors indicate whether the focal SGB is increasing or decreasing in its abundance over study visits, respectively. It then shows the average difference between patients with PFS ≥ 12 and PFS < 12 months across the different study visits. Non-gray cells in the heatmap correspond to the focal SGB's log-fold

change in abundance between patients with PFS ≥ 12 and PFS < 12 months, respectively. Teal cells correspond to study visits for which the abundance of the focal SGB is higher in patients with PFS ≥ 12 than with PFS < 12 months on monotherapy, and vice versa for brown cells (at 90% BCL). Gray cells denote differences between patients with PFS ≥ 12 and PFS < 12 months on monotherapy whose 90% CI overlapped with zero.



Extended Data Fig. 9 | Patients with PFS \geq 12 and PFS < 12 months on combination therapy. Panel (A) shows, for each microbial SGB listed, its slopes in patients with PFS \geq 12 months and PFS < 12 months on combination therapy, respectively. Red and blue colors indicate whether the focal SGB is increasing or decreasing in its abundance over study visits, respectively. It then shows the average difference between patients with PFS \geq 12 and PFS < 12 months across the different study visits. Non-gray cells in the heatmap correspond to the focal

SGB's log-fold change in abundance between patients with PFS \geq 12 and PFS < 12 months, respectively. Teal cells correspond to study visits for which the abundance of the focal SGB is higher in patients with PFS \geq 12 than with PFS < 12 months on combination therapy, and vice versa for brown cells (at 90% BCL). Gray cells denote differences between patients with PFS \geq 12 and PFS < 12 months on combination therapy whose 90% CI overlapped with zero.



Extended Data Fig. 10 | See next page for caption.

Extended Data Fig. 10 | Patients who developed and not developed colitis.

The figure shows, for each microbial SGB listed, its slopes in patients who developed and not developed colitis, respectively, regardless of response to therapy. Red and blue colors indicate whether the focal SGB is increasing or decreasing in its abundance over study visits, respectively. It then shows the average difference between patients with and without colitis across the different

study visits. Non-gray cells in the heatmap correspond to the focal SGB's log-fold change in abundance between patients with and without colitis, respectively. Teal cells correspond to study visits for which the abundance of the focal SGB is higher in patients who developed colitis compared to those resistant to colitis, and vice versa for brown cells (at 90% BCL). Gray cells denote differences between patients with and without colitis whose 90% CI overlapped with zero.

Reporting Summary

Nature Portfolio wishes to improve the reproducibility of the work that we publish. This form provides structure for consistency and transparency in reporting. For further information on Nature Portfolio policies, see our [Editorial Policies](#) and the [Editorial Policy Checklist](#).

Statistics

For all statistical analyses, confirm that the following items are present in the figure legend, table legend, main text, or Methods section.

n/a | Confirmed

- The exact sample size (n) for each experimental group/condition, given as a discrete number and unit of measurement
- A statement on whether measurements were taken from distinct samples or whether the same sample was measured repeatedly
- The statistical test(s) used AND whether they are one- or two-sided
Only common tests should be described solely by name; describe more complex techniques in the Methods section.
- A description of all covariates tested
- A description of any assumptions or corrections, such as tests of normality and adjustment for multiple comparisons
- A full description of the statistical parameters including central tendency (e.g. means) or other basic estimates (e.g. regression coefficient) AND variation (e.g. standard deviation) or associated estimates of uncertainty (e.g. confidence intervals)
- For null hypothesis testing, the test statistic (e.g. F , t , r) with confidence intervals, effect sizes, degrees of freedom and P value noted
Give P values as exact values whenever suitable.
- For Bayesian analysis, information on the choice of priors and Markov chain Monte Carlo settings
- For hierarchical and complex designs, identification of the appropriate level for tests and full reporting of outcomes
- Estimates of effect sizes (e.g. Cohen's d , Pearson's r), indicating how they were calculated

Our web collection on [statistics for biologists](#) contains articles on many of the points above.

Software and code

Policy information about [availability of computer code](#)

Data collection

Data taken from questionnaires, clinical visits and laboratory data from the majority of centres was collected on paper clinical report forms and entered using comma delimited files and excel spreadsheets. No specialist software was required. Exceptions were Oncolifes and POINTING studies. OncoLifes has used an UMCG-developed application called Utopia for data collection. (<https://www.ncbi.nlm.nih.gov/pmc/articles/PMC6857242/>)
Data within the POINTING cohort has been collected using the OpenClinica clinical trial software. (<https://www.openclinica.com/>)

Data analysis

Microsoft Excel version 2019
 MetaPhlAn v.4.0 (<https://github.com/biobakery/MetaPhlAn>)
 HUMAnN v.3.0 (<https://github.com/biobakery/humann>)
 fido (v.1.0.4) R package
 phyloseq (v.1.42.0) package
 tidyverse (v.2.0.0) package
 purrr (v.1.01) package
 caret (v.6.0-94) R package
 pROC (v.1.18.0) R package
 ggsurvfit (v.0.3.0) R package
 survival (v.3.5-5) R package

All code is available in the first author's GitHub page (<https://github.com/johannesbjork/Longitudinal-gut-microbiome-changes-in-ICB-treated-advanced-melanoma>)

For manuscripts utilizing custom algorithms or software that are central to the research but not yet described in published literature, software must be made available to editors and reviewers. We strongly encourage code deposition in a community repository (e.g. GitHub). See the Nature Portfolio [guidelines for submitting code & software](#) for further information.

Data

Policy information about [availability of data](#)

All manuscripts must include a [data availability statement](#). This statement should provide the following information, where applicable:

- Accession codes, unique identifiers, or web links for publicly available datasets
- A description of any restrictions on data availability
- For clinical datasets or third party data, please ensure that the statement adheres to our [policy](#)

The longitudinally profiled metagenomes have been deposited in the European Nucleotide Archive under accession number PRJEB70966. Baseline samples are already deposited under accession number PRJEB43119. All MetaPhlAn4 and HUMAnN3 profiles will also be available within the latest version of [curatedMetagenomicData](https://bioconductor.org/packages/curated/MetagenomicData) (<https://bioconductor.org/packages/curated/MetagenomicData>). All relevant patient data used in this study can be requested by emailing the first author (bjork.johannes@gmail.com). The six previously published studies used for validation are available under accession numbers: PRJNA770295; PRJNA541981; PRJNA762360; PRJNA399742; PRJNA397906; PRJEB22893, and PRJEB22894 (see Extended Data Table 1).

Research involving human participants, their data, or biological material

Policy information about studies with [human participants or human data](#). See also policy information about [sex, gender \(identity/presentation\), and sexual orientation](#) and [race, ethnicity and racism](#).

Reporting on sex and gender

Of the 175 patients, 75 were female and 100 male.

Reporting on race, ethnicity, or other socially relevant groupings

Ethnicity was not assessed

Population characteristics

Cohort characteristics are summarized in Table 1. We recruited 175 patients from five distinct cohorts across the Netherlands, the United Kingdom, and Spain treated with ICB for unresectable stage III and stage IV cutaneous melanoma, as previously described 4–10. One hundred seventeen (67%) patients received single agent treatment with an anti-programmed cell death (PD)-1 antibody (nivolumab or pembrolizumab), while 58 (33%) patients received combination therapy with anti-PD-1 and anti-cytotoxic T-lymphocyte-associated antigen (CTLA)-4 antibody (ipilimumab). The Response Evaluation Criteria in Solid Tumors (RECIST v.1.1) were used to determine tumor-response (Online methods). Clinical endpoints were defined as progression-free survival (PFS) at 12 months (PFS12) and overall survival (OS). PFS was defined as the time from the initial immunotherapy to disease progression or death, comparing patients achieving a PFS of 12 months or longer (PFS \geq 12) and patients with a PFS of less than 12 months (PFS<12). PFS12 was reached by 83 (47%) participants, and the overall median OS was 34.1 months (min=0.39 months, max=93.4 months; OS; censoring date, March 28, 2023). OS was defined for a subset of patients (n=147 patients) as the time in months from initiation of treatment to occurrence of death from any cause. Patients were followed over a maximum period of 7.3 years (median=4.3 years) after providing the first fecal sample. Fecal samples were collected at baseline and three subsequent treatment visits over a period of 12 weeks, Online methods, Figure S1).

Recruitment

We prospectively recruited 128 patients with advanced melanoma who were treated with ICB between August 2015 and January 2020 in the U.K. (PRIMM-UK, n=54) and the Netherlands (PRIMM-NL, n=74, made up of eligible patients from the COLIPI, POINTING and OncoLifeS studies). PRIMM-UK (NCT03643289) is sponsored by East & North Hertfordshire NHS Trust with ethical approval from King's College London. OncoLifeS (METc number 2010/109), COLIPI (METc number 2012/085, NCT02600143) and POINTING (METc number 2018/350, NCT04193956) have all been approved by the Medical Ethical Committee (in Dutch: Medisch Ethische Toetsingscommissie or METc) of the University Medical Center Groningen (UMCG) in the Netherlands. OncoLifeS information is available on the Netherlands Trial Register: NTR: <https://www.trialregister.nl/trial/7839>. Fecal samples were collected from these patients before initiation of ICB and longitudinally at up to four treatment (study) visits: at baseline and before each subsequent treatment cycle over a period of 12 weeks (Figure S1). The time between two samples was 3 or 4 weeks, depending on the treatment regimen, with ipilimumab/nivolumab combination therapy and pembrolizumab monotherapy administered 3-weekly and nivolumab monotherapy administered 4-weekly.

Patients who fulfilled the following criteria were eligible for the analysis: (i) histologically or cytologically confirmed non-

resectable advanced (stage III or IV) cutaneous melanoma, (ii) treatment with ICB (nivolumab or pembrolizumab) or a combination of ipilimumab and nivolumab at the recommended dose as a first-line ICI and (iii) 18 years of age or older and (iv) availability of baseline characteristics presented in Table 1.

Written informed consent was obtained from all patients.

Ethics oversight

King's College London (KCL); Medical Ethical Committee of the University Medical Center Groningen (METc UMCG); Manchester Cancer Research Centre (MCRC) Biobank Ethics and MCRC Biobank Access Committee; Ethical committee of Hospital Clinic of Barcelona.

Note that full information on the approval of the study protocol must also be provided in the manuscript.

Field-specific reporting

Please select the one below that is the best fit for your research. If you are not sure, read the appropriate sections before making your selection.

Life sciences Behavioural & social sciences Ecological, evolutionary & environmental sciences

For a reference copy of the document with all sections, see nature.com/documents/nr-reporting-summary-flat.pdf

Life sciences study design

All studies must disclose on these points even when the disclosure is negative.

Sample size

As this is an observational study, no power calculations were performed. From 447 samples from 195 patients, after quality control, SGB prevalence filtering and exclusion of samples with missingness in considered clinical metadata, we retained 408 samples from 175 patients.

Data exclusions

We excluded samples of participants with non-metastasized and resectable Stage III melanoma who received ICB's as adjuvant treatment. Moreover patients who were not immunotherapy-naïve were excluded. These exclusion criteria were established prior to this study. We also excluded patients who had any missingness in any of the considered confounder/predictor variables.

Replication

We replicated part of our results in six independent melanoma cohorts.

Randomization

As this was an observational cohort study randomization was not necessary or appropriate to produce our results and conclusions

Blinding

There was no control or placebo arm therefore blinding was not applicable

Reporting for specific materials, systems and methods

We require information from authors about some types of materials, experimental systems and methods used in many studies. Here, indicate whether each material, system or method listed is relevant to your study. If you are not sure if a list item applies to your research, read the appropriate section before selecting a response.

Materials & experimental systems

Methods

- n/a | Involved in the study
- Antibodies
- Eukaryotic cell lines
- Palaeontology and archaeology
- Animals and other organisms
- Clinical data
- Dual use research of concern
- Plants

- n/a | Involved in the study
- ChIP-seq
- Flow cytometry
- MRI-based neuroimaging

Clinical data

Policy information about [clinical studies](#)

All manuscripts should comply with the ICMJE [guidelines for publication of clinical research](#) and a completed [CONSORT checklist](#) must be included with all submissions.

Clinical trial registration

NCT02600143; NCT03643289; NCT04193956; <https://www.trialregister.nl/trial/7839>; MCRC 07/H1003/161+5 and MCRC 13_RIMA_01; HCB/2015/1032; REC Ref 15/NW/0933.

Study protocol

<https://www.clinicaltrials.gov>

Data collection

Patients within the PRIMM-cohorts were recruited in parallel, using aligned protocols 4. Additional patients, treated between March 2015 and November 2019, were enrolled from cohorts outside the setting of the PRIMM-study: Leeds (n=19); Barcelona (n=11) and Manchester (n=17). Fecal samples were collected at time points similar to those used in our included prospective studies. Patient

samples within the Manchester cohort were collected with written full-informed patient consent under Manchester Cancer Research Centre Biobank ethics application 07/H1003/161+5 (updated in 18/NW/0092) and approval for the work under Manchester Cancer Research Centre Biobank Access Committee application 13_RIMA_01. Barcelona cohort samples were subjected to the ethical committee of Hospital Clínic of Barcelona approval (registry HCB/2015/1032). Data and samples from Leeds were collected in a study named "Developing a blood test of immunity in illness: a study examining the peripheral blood transcriptome in patients with cancer, autoimmune disease, immunodeficiency or iatrogenic immune suppression" (Research Ethics Committee (REC) reference 15/NW/0933). Informed written consent was obtained for collection of samples and data, sharing anonymized data and working with collaborators whether academic or commercial.

Outcomes

Clinical endpoints were defined as progression-free survival (PFS) at 12 months (PFS12) and overall survival (OS). PFS was defined as the time from the initial immunotherapy to disease progression or death, comparing patients achieving a PFS of 12 months or longer ($PFS \geq 12$) and patients with a PFS of less than 12 months ($PFS < 12$). PFS12 was reached by 83 (47%) participants, and the overall median OS was 34.1 months (min=0.39 months, max=93.4 months; OS; censoring date, March 28, 2023). OS was defined for a subset of patients (n=147 patients) as the time in months from initiation of treatment to occurrence of death from any cause. Patients were followed over a maximum period of 7.3 years (median=4.3 years) after providing the first fecal sample. Fecal samples were collected at baseline and three subsequent treatment visits over a period of 12 weeks, Online methods, Figure S1).